nature geoscience

ARTICLES

https://doi.org/10.1038/s41561-020-00677-x

Check for updates

Enhanced aerosol particle growth sustained by high continental chlorine emission in India

Sachin S. Gunthe[1]✉, Pengfei Liu[2,3]✉, Upasana Panda[1,4], Subha S. Raj[1], Amit Sharma[1,16], Eoghan Darbyshire[5,17], Ernesto Reyes-Villegas[5], James Allan[5,6], Ying Chen[7,8], Xuan Wang[9], Shaojie Song[3], Mira L. Pöhlker[10], Liuhua Shi[11], Yu Wang[5], Snehitha M. Kommula[1], Tianjia Liu[12], R. Ravikrishna[13], Gordon McFiggans[5], Loretta J. Mickley[3], Scot T. Martin[3,12], Ulrich Pöschl[10], Meinrat O. Andreae[10,14,15] and Hugh Coe[5]

Many cities in India experience severe deterioration of air quality in winter. Particulate matter is a key atmospheric pollutant that impacts millions of people. In particular, the high mass concentration of particulate matter reduces visibility, which has severely damaged the economy and endangered human lives. But the underlying chemical mechanisms and physical processes responsible for initiating haze and fog formation remain poorly understood. Here we present the measurement results of chemical composition of particulate matter in Delhi and Chennai. We find persistently high chloride in Delhi and episodically high chloride in Chennai. These measurements, combined with thermodynamic modelling, suggest that in the presence of excess ammonia in Delhi, high local emission of hydrochloric acid partitions into aerosol water. The highly water-absorbing and soluble chloride in the aqueous phase substantially enhances aerosol water uptake through co-condensation, which sustains particle growth, leading to haze and fog formation. We therefore suggest that the high local concentration of gas-phase hydrochloric acid, possibly emitted from plastic-contained waste burning and industry, causes some 50% of the reduced visibility. Our work implies that identifying and regulating gaseous hydrochloric acid emissions could be critical to improve visibility and human health in India.

The 2018 World Air Quality Report mentioned New Delhi as the "world air pollution capital". In 2017–2018, particulate matter (PM) concentrations exceeded 200 μg m^{-3} and 600 μg m^{-3} for PM with diameter less than 1.0 μm and 2.5 μm, respectively (that is, PM_1 and $PM_{2.5}$)[1,2]. The severe pollution, also evidenced by high aerosol optical depth (AOD) over the Indo-Gangetic Plain (IGP; Fig. 1), is associated with increased respiratory and cardiovascular diseases, poor visibility and economic damages[3]. For example, persistent poor visibility over the New Delhi airport due to fog and haze has incurred significant financial losses to airline industries[4] and led to increasing vehicular deaths[3]. According to one estimate, in 2017 over Delhi alone, ~12,000 excess deaths can be attributed to exceedingly high $PM_{2.5}$ concentrations[5].

Numerous observational studies focusing on surface PM concentrations have been conducted over India during the past decade[2,6–17]. Although much progress has been made in measuring the seasonal variability of PM and its chemical composition, understanding of the underlying mechanisms responsible for the reduced visibility and deterioration of air quality over Delhi and the IGP remains limited. For example, it is unclear why the PM in Delhi has a higher potential to form haze and fog than in other polluted Asian cities[18], although a large fraction of Delhi PM is primary organic matter[2,19], which is less hygroscopic[20].

Here we present new chemical composition measurements of non-refractory PM smaller than 1 μm (NR-PM_1) from Delhi and a relatively cleaner Chennai (Fig. 1). Measurements are combined with thermodynamic modelling (Methods) to elucidate sources of the observed high chloride concentrations and the implications for PM concentrations and visibility. We report that high non-refractory particulate chloride in Delhi probably results from gas–particle partitioning of HCl gas into aerosol water under typical winter haze conditions of high relative humidity (RH), low temperatures and excess ammonia. The HCl is apparently emitted from continental anthropogenic sources, including industrial and combustion processes. In the process of co-condensation, the particulate chloride can take up more water, enhancing haze and fog formation. Our field observations and model calculations show that 50% visibility reduction in Delhi during the winter can be

[1]EWRE Division, Department of Civil Engineering, Indian Institute of Technology Madras, Chennai, India. [2]School of Earth and Atmospheric Sciences, Georgia Institute of Technology, Atlanta, GA, USA. [3]John A. Paulson School of Engineering and Applied Sciences, Harvard University, Cambridge, MA, USA. [4]Academy of Scientific and Innovative Research (AcSIR), Department of Environment and Sustainability, CSIR – Institute of Minerals and Materials Technology, Bhubaneswar, India. [5]Department of Earth and Environmental Sciences, School of Natural Sciences, University of Manchester, Manchester, UK. [6]National Centre for Atmospheric Science, University of Manchester, Manchester, UK. [7]Lancaster Environment Centre, Lancaster University, Lancaster, UK. [8]Data Science Institute, Lancaster University, Lancaster, UK. [9]School of Energy and Environment, City University of Hong Kong, Hong Kong SAR, China. [10]Multiphase Chemistry and Biogeochemistry Department, Max Planck Institute for Chemistry, Mainz, Germany. [11]Gangarosa Department of Environmental Health, Rollins School of Public Health, Emory University, Atlanta, GA, USA. [12]Department of Earth and Planetary Sciences, Harvard University, Cambridge, MA, USA. [13]Department of Chemical Engineering, Indian Institute of Technology Madras, Chennai, India. [14]Scripps Institution of Oceanography, University of California San Diego, La Jolla, CA, USA. [15]Department of Geology and Geophysics, King Saud University, Riyadh, Saudi Arabia. [16]Present address: Department of Civil and Infrastructure Engineering, Indian Institute of Technology Jodhpur, Karwar, Jodhpur, India. [17]Present address: The Conflict and Environment Observatory, Hebden Bridge, West Yorkshire, UK. ✉e-mail: s.gunthe@iitm.ac.in; pengfei.liu@eas.gatech.edu

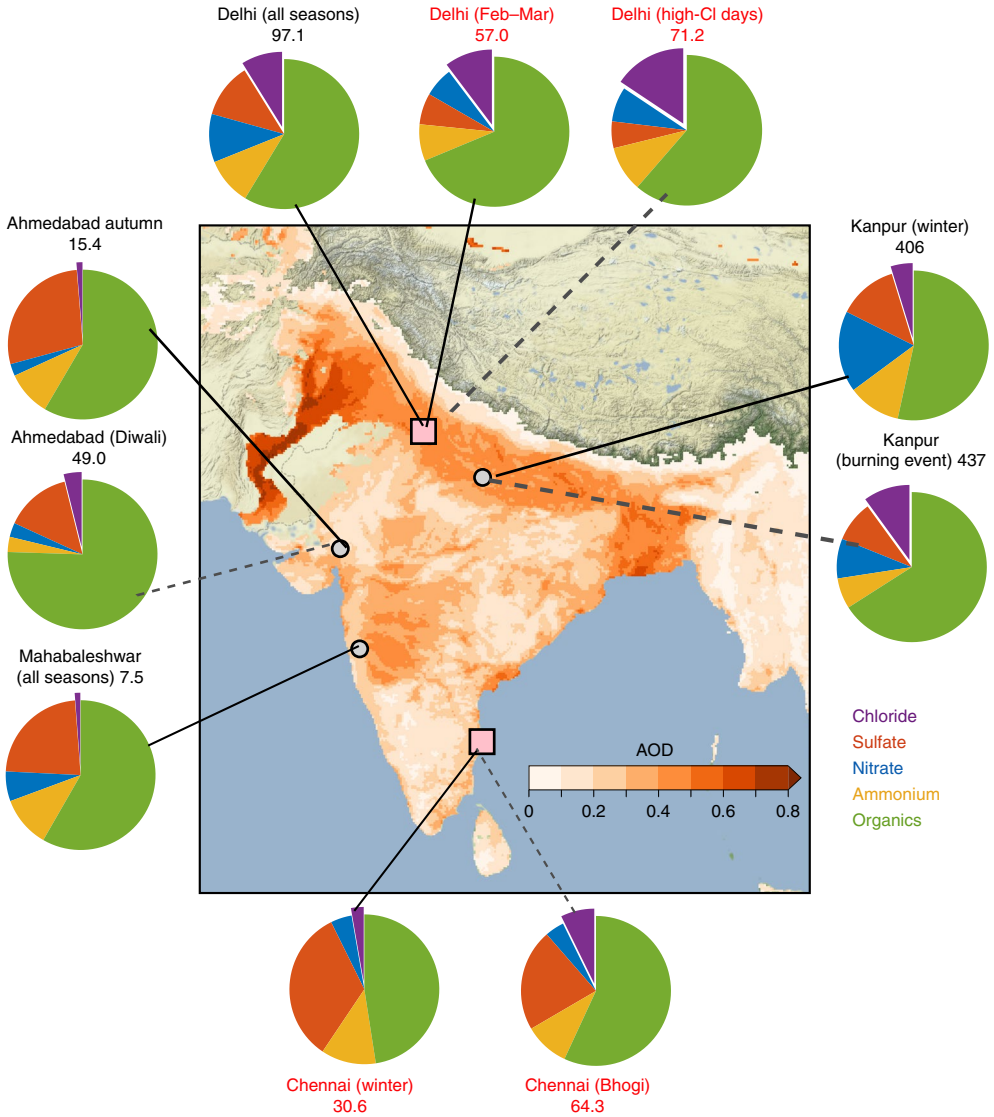

Fig. 1 | NR-PM_1 chemical components measured by aerosol mass spectrometer and ACSM over India. ACSM data are derived from this work (red text) and aerosol mass spectrometer data from literature (black text). Markers on the map show the measurement locations. Details of the measurement campaigns are summarized in Extended Data Fig. 1. The South Asia map is coded by orange colour for the annual mean (February 2018 to January 2019) of AOD derived from Moderate Resolution Imaging Spectroradiometer (MODIS). Pie charts represent different chemical species in NR-PM_1 for various locations over India connected by corresponding lines. Total mass concentrations of NR-PM_1 (in μg m^{-3}) are also marked for the respective pie charts. The pie charts represent the mass for all campaigns (connected by solid lines) and high-chloride episode, if present (connected by dashed lines).

attributed to the chloride co-condensation mechanism. In Chennai, high chloride concentrations in NR-PM_1 have been observed during the Bhogi festival, when bonfires are prevalent. The high levels of particulate chloride could participate in night-time multiphase chemistry producing reactive chlorine species, further affecting ozone and secondary organic aerosol (OA) production. These results highlight the uniqueness of atmospheric chemical processes in India, and suggest the importance of regulating chlorine anthropogenic sources.

Variations in PM_1 chemical composition over Delhi and Chennai

The chemical compositions of NR-PM_1 have been observed at diverse locations across India in the present study and literature[2,10,12,14,17] (Fig. 1 and Extended Data Figs. 1 and 2). Consistent with other global regions, OA comprised a major fraction of NR-PM_1. The chloride fraction, however, at least episodically remained an order of magnitude higher than the global average[21] over the IGP and metro cities. Notably, chloride comprises ~10% of NR-PM_1 mass in Delhi, which is comparable to other major inorganic components such as sulfate and nitrate. Several other studies using traditional sample-based techniques also reported a high chloride mass fraction in Delhi[9,19,22]. These high chloride fractions in NR-PM_1 observed over inland India are unexpected, as the dominant source of tropospheric chloride in NR-PM_1 was thought to be acid displacement mobilizing HCl from sea salt particles[23].

Figure 2 shows the time series of the NR-PM_1 chemical composition measured in Delhi and Chennai. Total NR-PM_1 reveals pronounced daily variations, with higher concentrations at night. At both sites, OA constitutes the largest mass fraction of total NR-PM_1 (69% and 48% for Delhi and Chennai, respectively). Factor analysis suggests that primary OA (POA)—that is, the sum

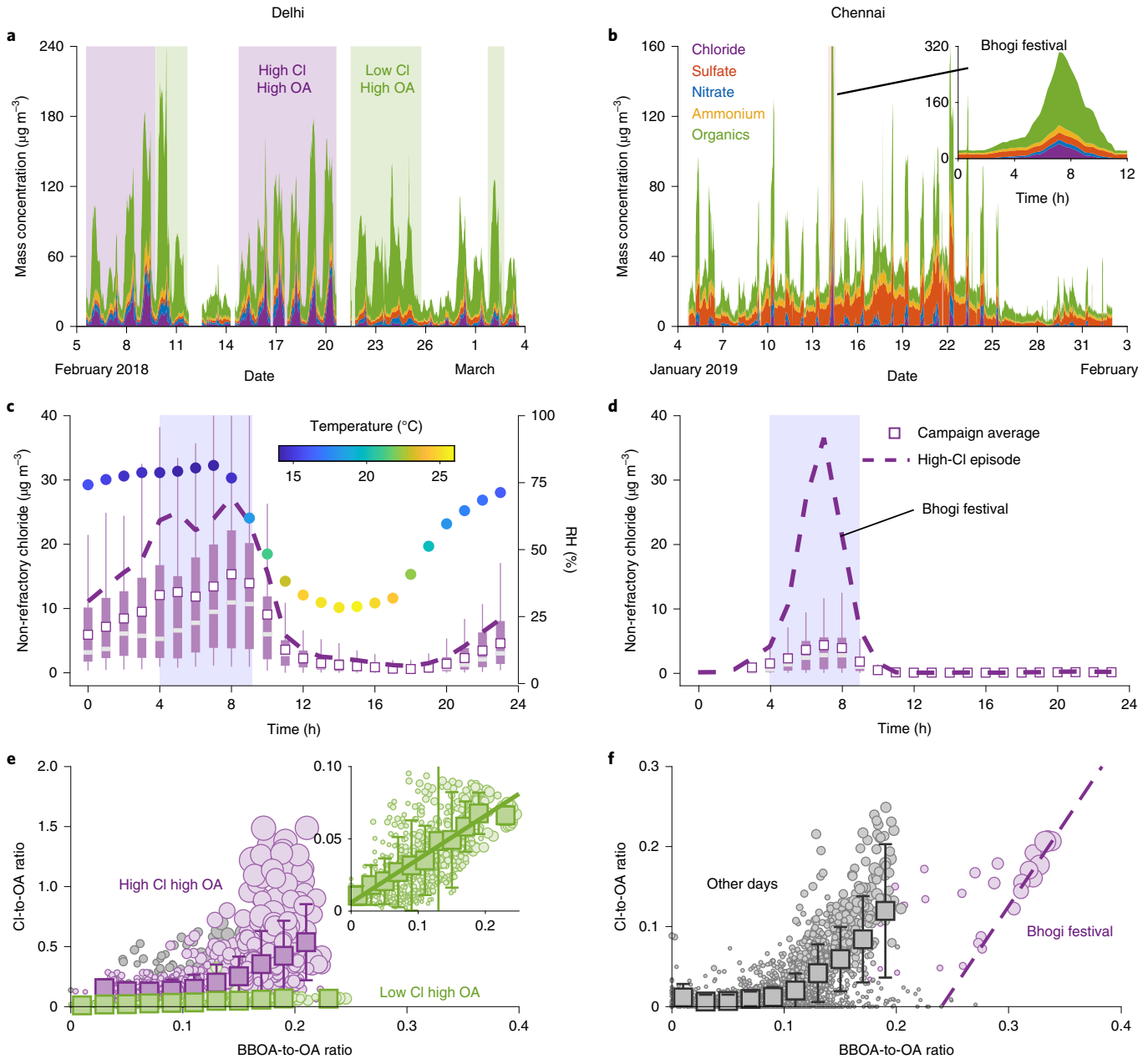

Fig. 2 | Time series of NR-PM$_1$, diel variations of chloride and scatter plots of Cl-to-OA versus BBOA-to-OA ratios over Delhi and Chennai. a,**b**, Time series of chemical components in NR-PM$_1$ measured during field campaigns in Delhi (**a**) and Chennai (**b**). Purple shading in **a** indicates the high-chloride and high-organics (P1) episode, and the green shading shows the low chloride and high organics (P2) periods. The inset in **b** shows the enhanced concentrations, particularly that of organics and chloride, during the Bhogi festival in Chennai on 14 January. **c**,**d**, Diel variations of chloride concentration for Delhi (**c**) and Chennai (**d**). The centre line and the box edges represent the median and quartiles for the dataset, respectively. Whiskers mark the highest and the lowest values that are within 1.5 times the interquartile range of the box edges. Open squares represent the mean values. Dashed lines show the mean diel variations for the high-chloride episodes. Diel variations of the temperature and RH in Delhi are also shown (**c**; right axis and colour bar). Purple shading indicates the values considered between 4:00 and 9:00 LT. **e**,**f**, Relationship between Cl-to-OA and BBOA-to-OA ratio for for Delhi (**e**) and Chennai (**f**). Inset in **e** shows the data from P2 days. Square markers and error bars represent mean and ±1 s.d.

of hydrocarbon-like OA (HOA), biomass burning OA (BBOA) and cooking OA (COA)—comprises 60% and 48% of the mass fraction of total OA for Delhi and Chennai, respectively (Methods and Extended Data Fig. 3), indicating a high contribution from open and domestic burning sources. Intermittent high chloride concentration occurs over Delhi, consistent with previous studies[2,19,22,24,25]. In Delhi, chloride constitutes the second-largest mass fraction of total NR-PM$_1$ (10.3%), higher than sulfate (6.8%) or nitrate (6.4%) (Extended Data Fig. 2). During the ten days of polluted episodes with high chloride and high OA in this study (P1; ~42% of total days in the campaign; light purple shaded areas in Fig. 2a), the daily mean mass fraction of chloride reaches 15.6% of NR-PM$_1$, higher than episodic values recorded elsewhere in India (Fig. 1 and Extended Data Fig. 1). In comparison, the daily mean chloride mass fraction remains at 3.7% during episodes of low chloride and high OA (P2; seven days, 25% of total campaign; light green shadings in Fig. 2a), comparable to the typical conditions in other polluted cities in India and China[26]. In Delhi, the NR-PM$_1$ chloride mass fraction is positively

associated with the total NR-PM_1 concentration, indicating enhanced contribution of chloride during highly polluted conditions (Extended Data Fig. 4). The highest chloride fraction averaged over the entire campaign occurs from 4:00 to 9:00 local time (LT; Fig. 2c and Extended Data Fig. 5), amounting 24% of NR-PM_1 for Delhi. High levels of chloride also occur in this time frame during P1. A plausible explanation is that these morning hours have the lowest temperatures and highest RH in a day, which favours the partitioning of gas-phase HCl to PM (Fig. 2c).

We hypothesize that the observed chloride in Delhi originates from a complex array of combustion sources and industrial processes. Among the identified OA factors, the BBOA fraction (that is, BBOA-to-OA ratio) correlates best with the chloride to OA (Cl-to-OA) ratio ($r=0.47$, $N=1977$; normalize by OA to eliminate the apparent correlation related to the diurnal variation of ventilation that simultaneously affects BBOA and Cl concentrations). During P2 days, the Cl-to-OA ratio linearly increases with the BBOA-to-OA ratio (Fig. 2e and the inset), indicating that chloride/HCl might be co-emitted with BBOA from biomass burning and biofuel combustion. During morning hours, when Cl is partitioning into the particle phase, the chloride to organic carbon (Cl-to-OC) and chloride to black carbon (Cl-to-BC) ratios are similar to the emission ratios of HCl-to-OC and HCl-to-BC reported for biomass burning and biofuel combustion (Extended Data Fig. 6). During P1, the overall positive correlation of Cl-to-OA ratio with BBOA-to-OA ratio suggests that combustion is still a persistent source of chloride. The Cl-to-OA and Cl-to-BC values, however, are comparable to the emission ratios reported for open burning of mixed rubbish[27–30], higher than that for burning of biomass and biofuels (Extended Data Fig. 6). An exponential increase during P1 in Cl-to-OA observed with respect to the BBOA-to-OA ratio indicates additional primary HCl sources. Results from the Stochastic Time-Inverted Lagrangian Transport (STILT) model suggest additional emissions may come from industries located north–northwest of the observational site (Methods and Extended Data Fig. 7). A large number of illegal, informal and unorganized metal processing units, as well as e-waste recycling and handling units, plastic processing units and medical waste management facilities, are widespread in that area (Extended Data Fig. 7), and the use of acids by these industries[31–36] may contribute to the direct HCl gas emissions.

In contrast, in Chennai, even though it is located on the coast, chloride on average constituted just 2.7% of total NR-PM_1. However, on 14 January 2019, the Bhogi festival took place there, causing chloride concentrations to reach 40 μg m^{-3} during the night, corresponding to 11% of total NR-PM_1 (Fig. 2b,d and Extended Data Fig. 3). During Bhogi, large-scale burning of wood logs, solid waste and wooden furniture takes place, following an old and important tradition (ref. [37] and Methods). The solid waste burned contains a significant amount of plastics, such as polyvinyl chloride, and burning of such waste releases HCl gas[38], which can then partition into the aqueous particle phase[39]. We find a strong linear relationship between the BBOA-to-OA ratio and the Cl-to-OA ratio (Fig. 2f), indicating increased chloride concentration from combustion of mixed wood and solid waste in Chennai. Other than during the Bhogi festival, the campaign-averaged chloride level in Chennai was lower than the observed average in Delhi, most probably due to lower HCl emissions and less favourable meteorological conditions—that is, higher temperatures and lower RH compared with Delhi (Extended Data Fig. 2). Similarly, enhanced chloride concentrations were also observed in Ahmedabad during the Diwali festival, and in Kanpur during a high-biomass-burning event[10,12,14] (Fig. 1).

Thermodynamic modelling

The observed chloride in NR-PM_1 is generally in the form of ammonium chloride[23,40], produced by the reaction of NH_3 in the atmosphere with direct HCl emissions[41,42]. Figure 3a shows that sulfate and nitrate, the predominant inorganic species of fine PM in most regions, account for only 50% of the inorganic anions in Delhi PM. Chloride, as the single largest inorganic anion in Delhi PM, neutralized 50% of ammonium, on par with sulfate and nitrate combined. The refractory forms of chloride, such as sodium chloride from sea salt and potassium chloride from biomass burning, are not included here because these species do not vapourize at 600 °C, which is a requirement of the instrumentation used here (that is, the mass spectrometer vapourizer). From a global budget perspective, acid displacement and heterogeneous reactions on sea salt particles is a major source of HCl[43]. In the IGP, however, it is highly unlikely that marine-originated chlorine sources can contribute significantly to HCl and non-refractory chloride.

To further explain the unique thermodynamic nature of the chloride-rich Delhi PM, we analysed the observed aerosol composition, RH and temperature with the thermodynamic model ISORROPIA II[44] (Methods). For a sensitivity analysis of chemical conditions, the predicted equilibrium fraction of Cl in the particle phase (that is, $Cl^-/(Cl^- + HCl)$) across different concentrations of total sulfuric acid and ammonia is shown in Fig. 3b. Three distinct regimes of the aqueous fraction of chloride were identified, suggesting a high fraction of Cl in the particle phase is strongly dependent on the presence of excess ammonia in the atmosphere. Previous studies have reported high gas-phase ammonia concentrations over Delhi (~30 μg m^{-3}; shown by the green box in Fig. 3b[45]), indicating an ammonia excess regime explaining high chloride concentrations in our observations. In the chemical regime of Delhi, decreasing the sulfate concentration would marginally reduce particle-phase chloride, mainly because of the decrease in sulfate-associated liquid water. Ammonia seems to be a controlling factor for chloride partitioning. To decrease the particle-phase Cl fraction, however, an aggressive ammonia emission reduction would be required (more than 50% reduction in total ammonium), a difficult task as in India it is largely emitted from agricultural sources, including livestock and fertilizer use. Reducing the anthropogenic sources of HCl appears to be the only feasible approach to effectively control the particle-phase chloride concentration.

Both the PM chloride concentration and chloride fraction in NR-PM_1 show strong temperature and RH dependence (Extended Data Fig. 8). To explain these behaviours, we performed thermodynamic calculations for a wide range of temperature and RH values (Fig. 3c). For the observed range of temperature (10–18 °C) and RH (70–85%) during morning hours (4:00–9:00 LT) over Delhi, the predicted fraction of Cl in the particle phase ranged from 80% to 99%. By comparison, during afternoon hours (14:00–18:00 LT), this fraction was consistently less than 30%. The contrast in the partitioning behaviour for different hours of the day was driven by changes in both PM-associated liquid water and ambient temperature. These results are consistent with the observations showing that the chloride content of NR-PM_1 was high during morning hours and decreased substantially in the afternoon (Extended Data Fig. 5). Besides the thermodynamically driven partitioning, other factors, such as shallow boundary layer during early morning hours, which cannot explain the increase of chloride mass fraction, can further enhance the concentrations of chloride and other PM species, causing severe visibility reduction at this time of day.

The measurements indicate a strong correlation between chloride and liquid water content of PM over a wide range of RH and PM mass concentrations (Fig. 3d). This positive correlation is in line with the model prediction indicating co-condensation of chloride occurs along with water uptake (Extended Data Fig. 9 and red dashed line in Fig. 3d). Co-condensation has been reported previously for organic vapours[46] and nitric acid[47], using parameterizations and modelling approaches primarily concluding that water-soluble and semi-volatile species, such as organic vapours and nitric acid, can significantly enhance the water uptake and cloud activation

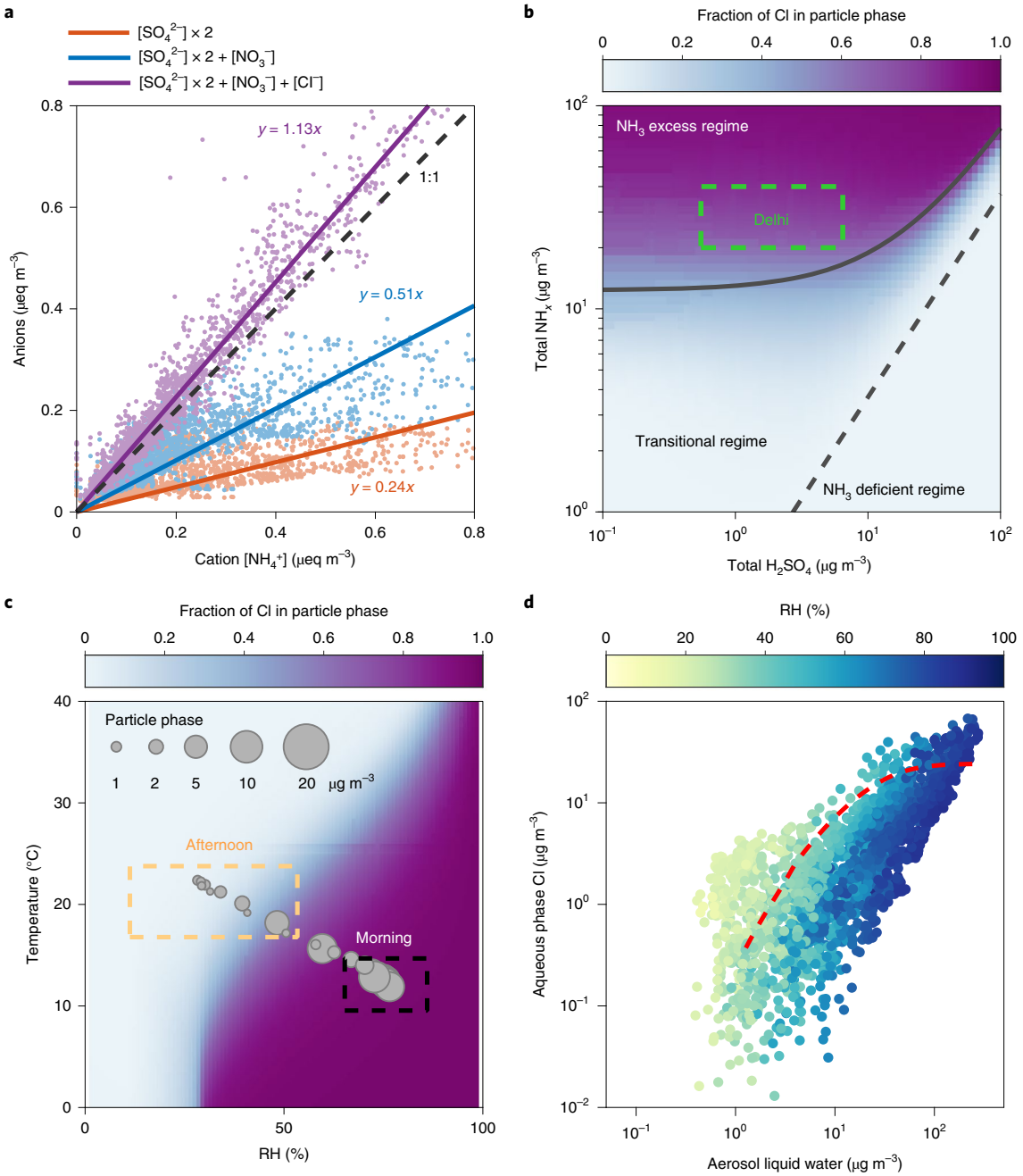

Fig. 3 | Thermodynamic modelling of the gas–particle partitioning of chloride in Delhi. a, Ion balance of NR-PM_1 in Delhi measured by the ACSM. The coloured lines indicate anion-to-cation ratios for sulfate (red), sulfate + nitrate (blue) and sulfate + nitrate + chloride (purple), and the black dashed line denotes 1:1. **b**, Fraction of chloride in the particle phase as a function of total ammonium (gas phase + particle phase) and total sulfate modelled by the thermodynamic model, assuming the aerosol adopts a metastable state. The simulations used a campaign-averaged RH of 57% and temperature of 17 °C for Delhi. Total nitrate was assumed to increase with increasing total sulfate, with a mass ratio of 1:1, consistent with the measurements in Delhi. A total chloride concentration of 25 μg m^{-3} was used in the simulations. Typical total ammonium and total sulfate values of Delhi, as inferred from the literature[32] and the field measurements of this study, are marked by the green box. The dashed line represents the condition in which the total ammonia is neutralized by sulfate $n(NH_x) = 2\,n(SO_4^{2-})$. The solid curve represents the condition in which the total ammonia is fully neutralized by sulfate, nitrate and chloride, that is, $n(NH_x) = 2\,n(SO_4^{2-}) + n(NO_3^-) + n(Cl^-)$. **c**, Modelled aqueous fraction of chloride as a function of temperature and RH. The points show the measured particle-phase chloride concentrations during the high-chloride episodes as a function of temperature and RH. The boxes indicate conditions of morning and afternoon hours during the field campaign in Delhi. **d**, Measured particle-phase chloride as a function of aerosol liquid water derived from model (Methods section). The red dashed line shows the increase of the modelled particle-phase chloride with an increasing RH from 15% to 90% (Extended Data Fig. 9), assuming total Cl (Cl^- + HCl) is 25 μg m^{-3}. The PM liquid water associated with inorganics was calculated using the ISORROPIA II model in reverse mode based on the ACSM measured chemical composition. The aerosol liquid water associated with organics was calculated using a hygroscopicity parameter $\kappa = 0.1$ (refs. [20,49]).

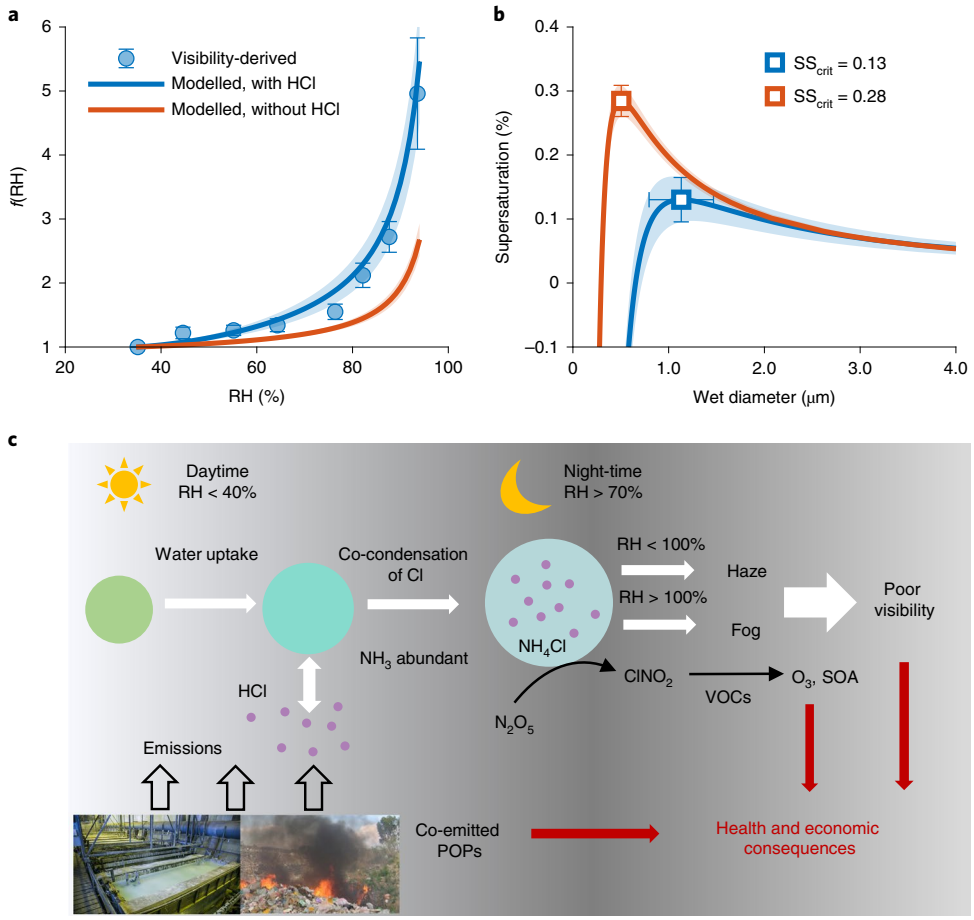

Fig. 4 | The impact of chloride co-condensation on PM hygroscopic growth and cloud/fog formation. a, *f*(RH) calculated based on observed visibility and $PM_{2.5}$ measurements and modelled using ISORROPIA II. Blue circles represent the calculated *f*(RH) based on visibility and $PM_{2.5}$ (ref. [18]). Error bars represent the uncertainty estimated using bootstrapping. Blue and red curves represent the *f*(RH) modelled using ISORROPIA II with and without consideration of chloride, respectively (see Methods). **b**, Köhler curves calculated with and without the co-condensation of chloride. Critical supersaturation values (SS_{crit}) are labelled. Shaded regions in **a** and **b**, and error bars in **b**, represent the uncertainty in model-derived parameters calculated using Monte Carlo simulations. **c**, Schematic showing the HCl emission from rubbish burning and industrial sources, co-condensation of chloride, and the possible influences on haze and fog formation. Other potential environmental impacts, such as the influence on ozone chemistry and co-emission of POPs, are also depicted.

tendency of atmospheric PM. The gas–particle partitioning of HCl and NH_4Cl experiences a similar co-condensation process as organic vapours and nitric acid, but causes a greater increase in hygroscopicity of particles. Ambient in situ observations indeed confirm that PM in Delhi exhibits higher water uptake capability than another polluted megacity, Beijing[18], consistent with this study. This high hygroscopicity is unexpected based on conventional understanding due to high organic mass fraction (60–70%) of the NR-PM_1 in Delhi, higher than the typical value of 40–50% in polluted Beijing[48]. A higher organic fraction, which is less hygroscopic than inorganic salts, is typically associated with lower hygroscopicity[20].

Here we show that chloride co-condensation can explain the observed high hygroscopicity of Delhi PM. Following the method described by ref. [18], we derived the aerosol light-extinction enhancement factor *f*(RH) in Delhi based on ambient measurements of visibility and $PM_{2.5}$ (Methods). The visibility provides a direct measure of light extinction under ambient conditions. The *f*(RH) represents the ratio of the mass extinction coefficient at elevated RH to that at dry conditions (RH < 35%). This approach is found to be most suitable to investigate co-condensation effect as it does not perturb the concentrations of soluble gases such as HCl, HNO_3 and NH_3, which otherwise may get evaporated during the measurements owing to conditioning of air samples.

Role of high chloride in visibility reduction

The visibility-derived *f*(RH) values were compared with the thermodynamic results (Fig. 4a). Two modelling cases were formulated to illustrate the effect of chloride co-condensation (Methods). In the modelled case considering chloride co-condensation, a total chloride concentration of 25 μg m^{-3} (gas phase + particle phase, HCl equivalent) was used (blue curve in Fig. 4a). The model yields a change in particle composition, which causes a light-extinction enhancement that is consistent with the measurements (Extended Data Fig. 9). The reference case (red curve) considers a chloride-free environment—that is, the total chloride concentration was set to zero. For both cases, the RH values were varied from <35% to >90%, and the equilibrium partitioning of water and semi-volatile species between gas and particle phases was calculated. The model results agree well with the observed *f*(RH) when chloride was included in the model, whereas in the case without chloride, the modelled *f*(RH) is biased low compared with measurements. For RH from 90% to 95%, which consistently occurs over Delhi during winter haze episodes, a high value of 5 for *f*(RH) indicates a strong water uptake by PM. For RH

values beyond 95%, f(RH) values are expected to be much higher than the value of 5 as reported here, comparable to the hygroscopicity of pure ammonium sulfate[49]. At a similar RH level, the modelled f(RH) without accounting for chloride has a smaller value of 2.5. Thus, presence of HCl can strongly enhance water uptake through co-condensation into the PM, contributing to ~50% of the visibility degradation during the haze/fog events.

We also show that the co-condensation mechanism can lower the barrier of cloud activation[47], thus promoting fog/cloud formation. The cloud condensation nuclei (CCN) activation of typically sized particles was calculated by combining the thermodynamic model with the Kelvin effect to calculate the Köhler curves (Methods). Figure 4b shows the effect of higher HCl concentration in the atmosphere on the equilibrium supersaturation ratios. Particles with 100 nm dry diameter have full CCN activation at a critical supersaturation of 0.13%, and a factor of 2 lower when the atmosphere is considered without chloride (that is, 0.28%). This indicates a strong cloud activation capability of PM over Delhi at times when chloride is abundant. The enhanced particle growth encompassing a wide range of water vapour concentration (from sub- to supersaturated range) corresponds with the period from late evening to early morning, an intense fog formation period over Delhi.

In summary, these analyses examine the complex chemical and physical processes and underlying mechanisms related to reduced visibility in Delhi, which have large negative consequences on the economy and societal well-being. We find that water uptake and fog formation are significantly increased by co-condensation processes involving semi-volatile species, especially chloride (Fig. 4c). In the presence of abundant ammonia and at high RH, the gas-phase HCl co-condenses with water into the PM to form NH_4Cl, significantly enhancing particle light scattering. The widespread burning of diverse, significant and unaccounted waste including plastic, and processing of e-waste combined with primary emissions from various industrial sources[32,34,50] throughout Delhi, probably represent a large but not yet well-quantified HCl source.

In addition to the deterioration of visibility, the chlorine-rich atmosphere in India represents other environmental implications. For example, burning of chlorine-containing plastics, as present in e-waste, can emit a large amount of dioxins and other persistent organic pollutants (POPs[50]) that are highly toxic and can accumulate in the food chain (Fig. 4c). Gaseous and particulate chloride can also affect atmospheric chemistry in other ways[23]. In a polluted environment containing these species, the aqueous-phase reaction of chloride with N_2O_5 at night-time extends the NO_x lifetime producing nitryl chloride ($ClNO_2$), which in turn photolyses during daytime, enhancing ozone and PM production via Cl atom pathways[51–54]. The oxidation pathways over India thus may be significantly different from other continental regions due to high HCl concentrations. Additional measurements are required to explore the scale, sources and significance of HCl emissions. While the role of HCl emissions reported here is important in controlling water uptake and visibility reduction, we emphasize the need for continued efforts by policymakers in reducing the key precursors and major primary sources of particulate pollution, including ammonia emissions from agriculture, burning of crop residue, biofuel combustion, emissions from coal-fired power plants, small-scale processing industries and automobiles. We emphasize the urgency for systematic and long-term measurements of PM composition (refractory and non-refractory) and hygroscopicity, as well as those of gas-phase HCl, ozone and POPs, to better understand their role in regional climate, atmospheric chemistry, visibility degradation and human health in India. These findings may help frame overall better policies to synergistically tackle the concurrent environmental issues in India, including air pollution, solid-waste management comprising e-waste and food safety. Strong regulation on open waste dumping and burning and on industrial chlorine emissions appears to be necessary.

Online content

Any methods, additional references, Nature Research reporting summaries, source data, extended data, supplementary information, acknowledgements, peer review information; details of author contributions and competing interests; and statements of data and code availability are available at https://doi.org/10.1038/s41561-020-00677-x.

Received: 20 August 2020; Accepted: 1 December 2020;
Published online: 25 January 2021

References

1. Beig, G. et al. Anatomy of the winter 2017 air quality emergency in Delhi. *Sci. Total Environ.* **681**, 305–311 (2019).
2. Gani, S. et al. Submicron aerosol composition in the world's most polluted megacity: the Delhi Aerosol Supersite study. *Atmos. Chem. Phys.* **19**, 6843–6859 (2019).
3. Dey, S. On the theoretical aspects of improved fog detection and prediction in India. *Atmos. Res.* **202**, 77–80 (2018).
4. Kulkarni, R. et al. Loss to aviation economy due to winter fog in New Delhi during the winter of 2011–2016. *Atmosphere* **10**, 198 (2019).
5. Balakrishnan, K. et al. The impact of air pollution on deaths, disease burden, and life expectancy across the states of India: the Global Burden of Disease Study 2017. *Lancet Planet. Health* **3**, e26–e39 (2019).
6. Balachandran, S., Meena, B. R. & Khillare, P. S. Particle size distribution and its elemental composition in the ambient air of Delhi. *Environ. Int.* **26**, 49–54 (2000).
7. Cheng, Z. et al. Status and characteristics of ambient $PM_{2.5}$ pollution in global megacities. *Environ. Int.* **89–90**, 212–221 (2016).
8. Monkkonen, P. et al. Relationship and variations of aerosol number and PM_{10} mass concentrations in a highly polluted urban environment – New Delhi, India. *Atmos. Environ.* **38**, 425–433 (2004).
9. Pant, P. et al. Characterization of ambient $PM_{2.5}$ at a pollution hotspot in New Delhi, India and inference of sources. *Atmos. Environ.* **109**, 178–189 (2015).
10. Rastogi, N., Singh, A. & Satish, R. Characteristics of submicron particles coming from a big firecrackers burning event: implications to atmospheric pollution. *Atmos. Pollut. Res.* **10**, 629–634 (2019).
11. Saxena, M. et al. Water soluble inorganic species of PM_{10} and $PM_{2.5}$ at an urban site of Delhi, India: seasonal variability and sources. *Atmos. Res.* **184**, 112–125 (2017).
12. Singh, A., Satish, R. V. & Rastogi, N. Characteristics and sources of fine organic aerosol over a big semi-arid urban city of western India using HR-ToF-AMS. *Atmos. Environ.* **208**, 103–112 (2019).
13. Srivastava, A., Gupta, S. & Jain, V. K. Source apportionment of total suspended particulate matter in coarse and fine size ranges over Delhi. *Aerosol Air Qual. Res.* **8**, 188–200 (2008).
14. Thamban, N. M. et al. Evolution of aerosol size and composition in the Indo-Gangetic Plain: size-resolved analysis of high-resolution aerosol mass spectra. *ACS Earth Space Chem.* **3**, 823–832 (2019).
15. Tiwari, S. et al. Black carbon and chemical characteristics of PM_{10} and $PM_{2.5}$ at an urban site of north India. *J. Atmos. Chem.* **62**, 193–209 (2009).
16. Yadav, S. & Rajamani, V. Air quality and trace metal chemistry of different size fractions of aerosols in N-NW India – implications for source diversity. *Atmos. Environ.* **40**, 698–712 (2006).
17. Mukherjee, S. et al. Seasonal variability in chemical composition and source apportionment of sub-micron aerosol over a high altitude site in Western Ghats, India. *Atmos. Environ.* **180**, 79–92 (2018).
18. Wang, Y. & Chen, Y. Significant climate impact of highly hygroscopic atmospheric aerosols in Delhi, India. *Geophys. Res. Lett.* **46**, 5535–5545 (2019).
19. Jaiprakash, S. A., Habib, G., Raman, R. S. & Gupta, T. Chemical characterization of $PM_{1.0}$ aerosol in Delhi and source apportionment using positive matrix factorization. *Environ. Sci. Pollut. Res.* **24**, 445–462 (2017).
20. Gunthe, S. S. et al. Cloud condensation nuclei in pristine tropical rainforest air of Amazonia: size-resolved measurements and modeling of atmospheric aerosol composition and CCN activity. *Atmos. Chem. Phys.* **9**, 7551–7575 (2009).
21. Zhang, Q. et al. Ubiquity and dominance of oxygenated species in organic aerosols in anthropogenically-influenced Northern Hemisphere midlatitudes. *Geophys. Res. Lett.* **34**, L13801 (2007).
22. Kumar, B., Chakraborty, A., Tripathi, S. N. & Bhattu, D. Highly time resolved chemical characterization of submicron organic aerosols at a polluted urban location. *Environ. Sci. Process. Impacts* **18**, 1285–1296 (2016).

23. Wang, X. et al. The role of chlorine in global tropospheric chemistry. *Atmos. Chem. Phys.* **19**, 3981–4003 (2019).
24. Kapoor, R. K. & Murty, B. V. R. Sulphate aerosol at Delhi in relation to the associated chloride component. *J. Appl. Meteorol.* **5**, 493–499 (1966).
25. Perrino, C. et al. Chemical characterization of atmospheric PM in Delhi, India, during different periods of the year including Diwali festival. *Atmos. Pollut. Res.* **2**, 418–427 (2011).
26. Song, S. et al. Thermodynamic modeling suggests declines in water uptake and acidity of inorganic aerosols in Beijing winter haze events during 2014/2015–2018/2019. *Environ. Sci. Technol. Lett.* **6**, 752–760 (2019).
27. Akagi, S. K. et al. Emission factors for open and domestic biomass burning for use in atmospheric models. *Atmos. Chem. Phys.* **11**, 4039–4072 (2011).
28. Christian, T. J. et al. Trace gas and particle emissions from domestic and industrial biofuel use and garbage burning in central Mexico. *Atmos. Chem. Phys.* **10**, 565–584 (2010).
29. Lemieux, P. M., Lutes, C. C., Abbott, J. A. & Aldous, K. M. Emissions of polychlorinated dibenzo-p-dioxins and polychlorinated dibenzofurans from the open burning of household waste in barrels. *Environ. Sci. Technol.* **34**, 377–384 (2000).
30. Andreae, M. O. Emission of trace gases and aerosols from biomass burning – an updated assessment. *Atmos. Chem. Phys.* **19**, 8523–8546 (2019).
31. Chakraborty, P. et al. Baseline investigation on plasticizers, bisphenol A, polycyclic aromatic hydrocarbons and heavy metals in the surface soil of the informal electronic waste recycling workshops and nearby open dumpsites in Indian metropolitan cities. *Environ. Pollut.* **248**, 1036–1045 (2019).
32. Chakraborty, P. et al. PCBs and PCDD/Fs in soil from informal e-waste recycling sites and open dumpsites in India: levels, congener profiles and health risk assessment. *Sci. Total Environ.* **621**, 930–938 (2018).
33. Chakraborty, P. et al. Passive air sampling of polybrominated diphenyl ethers in New Delhi, Kolkata, Mumbai and Chennai: levels, homologous profiling and source apportionment. *Environ. Pollut.* **231**, 1181–1187 (2017).
34. Nagpure, A. S. Assessment of quantity and composition of illegal dumped municipal solid waste (MSW) in Delhi. *Resour. Conserv. Recycl.* **141**, 54–60 (2019).
35. Pradhan, J. K. & Kumar, S. Informal e-waste recycling: environmental risk assessment of heavy metal contamination in Mandoli industrial area, Delhi, India. *Environ. Sci. Pollut. Res.* **21**, 7913–7928 (2014).
36. Salam, M. & Varma, A. Bacterial community structure in soils contaminated with electronic waste pollutants from Delhi NCR, India. *Electron. J. Biotechnol.* **41**, 72–80 (2019).
37. Suresh, R., Janakiramayya, M. V. & Sukumar, E. R. An account of fog over Chennai. *Mausam* **58**, 501–512 (2007).
38. Stockwell, C. E. et al. Nepal Ambient Monitoring and Source Testing Experiment (NAMaSTE): emissions of trace gases and light-absorbing carbon from wood and dung cooking fires, garbage and crop residue burning, brick kilns, and other sources. *Atmos. Chem. Phys.* **16**, 11043–11081 (2016).
39. Fu, X. et al. Anthropogenic emissions of hydrogen chloride and fine particulate chloride in China. *Environ. Sci. Technol.* **52**, 1644–1654 (2018).
40. Saiz-Lopez, A. & von Glasow, R. Reactive halogen chemistry in the troposphere. *Chem. Soc. Rev.* **41**, 6448–6472 (2012).
41. Andreae, M. O. et al. Airborne studies of aerosol emissions from savanna fires in southern Africa: 2. Aerosol chemical composition. *J. Geophys. Res. Atmos.* **103**, 32119–32128 (1998).
42. Goetz, J. D. et al. Speciated online PM_1 from South Asian combustion sources – Part 1: fuel-based emission factors and size distributions. *Atmos. Chem. Phys.* **18**, 14653–14679 (2018).
43. Finlayson-Pitts, B. J. The tropospheric chemistry of sea salt: a molecular-level view of the chemistry of NaCl and NaBr. *Chem. Rev.* **103**, 4801–4822 (2003).
44. Fountoukis, C. & Nenes, A. ISORROPIA II: a computationally efficient thermodynamic equilibrium model for K^+-Ca^{2+}-Mg^{2+}-Nh_4^+-Na^+-SO_4^{2-}-NO_3^--Cl^--H_2O aerosols. *Atmos. Chem. Phys.* **7**, 4639–4659 (2007).
45. Singh, S. & Kulshrestha, U. C. Abundance and distribution of gaseous ammonia and particulate ammonium at Delhi, India. *Biogeosciences* **9**, 5023–5029 (2012).
46. Topping, D., Connolly, P. & McFiggans, G. Cloud droplet number enhanced by co-condensation of organic vapours. *Nat. Geosci.* **6**, 443–446 (2013).
47. Kulmala, M., Laaksonen, A., Charlson, R. J. & Korhonen, P. Clouds without supersaturation. *Nature* **388**, 336–337 (1997).
48. Hu, W. W. et al. Chemical composition, sources, and aging process of submicron aerosols in Beijing: contrast between summer and winter. *J. Geophys. Res. Atmos.* **121**, 1955–1977 (2016).
49. Petters, M. D. & Kreidenweis, S. M. A single parameter representation of hygroscopic growth and cloud condensation nucleus activity. *Atmos. Chem. Phys.* **7**, 1961–1971 (2007).
50. Verma, R., Vinoda, K. S., Papireddy, M. & Gowda, A. N. S. Toxic pollutants from plastic waste - a review. *Procedia Environ. Sci.* **35**, 701–708 (2016).
51. Behnke, W., George, C., Scheer, V. & Zetzsch, C. Production and decay of $ClNO_2$, from the reaction of gaseous N_2O_5 with NaCl solution: bulk and aerosol experiments. *J. Geophys. Res. Atmos.* **102**, 3795–3804 (1997).
52. Cai, X. & Griffin, R. J. Secondary aerosol formation from the oxidation of biogenic hydrocarbons by chlorine atoms. *J. Geophys. Res. Atmos.* **111**, D14206 (2006).
53. Osthoff, H. D. et al. High levels of nitryl chloride in the polluted subtropical marine boundary layer. *Nat. Geosci.* **1**, 324–328 (2008).
54. Thornton, J. A. et al. A large atomic chlorine source inferred from mid-continental reactive nitrogen chemistry. *Nature* **464**, 271–274 (2010).

Methods

Sampling sites. *Delhi.* The aerosol sampling in Delhi was conducted at the Indian Meteorological Department campus (28.59° N, 77.22° E; 200 m above sea level) during February–March 2018 using advanced instrumentation under the Atmospheric Pollution and Human Health Program of the Process Analysis, Observations and Modelling—Integrated Solutions for Cleaner Air for Delhi (APHH-PROMOTE) campaign. All the instruments were placed in an air-conditioned container connected to a dedicated inlet with a sampling height of ~5 m above the ground. The inlet was constructed of stainless steel with a cyclone separator and with proper protection, to avoid any blockage in the inlet. The air sampled can be considered as representative of the region in view of the average time and duration of the sampling. Briefly, the capital city of India—considered to be one of the most populated and polluted cities in the world—experiences very diverse climatic conditions. The winters, from December to February are mildly cold (with average diurnal temperatures of 5–20 °C) and humid (average diurnal RH of 45–95%). During the winter season, owing to frequent inversions, the boundary layer depth is generally less than 100 m, especially during early morning hours before sunrise, when the temperature reaches its minimum. During the winter season, Delhi experiences very high aerosol mass burdens attributed to local emissions and regional transport[1].

The sampling site is surrounded by small- and medium-scale industries within a 25 km vicinity, dealing with metal processing, paper production, plastic and medicine manufacturing, e-waste handling and recycling, medical waste management, dumping sites management and so on, which cause emissions of various toxic gases and pollutants into the atmosphere of Delhi[11,19,31–35,50,55]. According to an estimate, on average 606 Mg km^{-2} of municipal solid waste (MSW) are illegally dumped in Delhi, resulting 557,000 Mg of MSW lying on streets and open areas, including 38,000 Mg of plastic[34]. Delhi experiences open burning of 216,000 Mg of MSW per year[56], some of which occurs at non-designated places and also ends up as fuel for brick kilns[42]. This waste mainly constitutes diverse rubbish, but a common and abundant component is mixed plastic from food wrappers and e-waste. Large numbers of informal and unorganized units for e-waste handling and recycling, and metal processing, are prevalent across Delhi[34] (Extended Data Fig. 7). E-waste handling units aim to retrieve copper, silver and gold from printed circuit boards, cables, scrap plastics and batteries with processes that use acids and open burning. The metal processing industries use acids for pickling and polishing purposes. Interestingly, HCl is widely used in the steel processing industries for pickling to remove iron oxides and scale from the surface of steel. In metal industries, HCl is also widely used for aluminium etching, metal cleansing and metal pre-fixing. These processes are known to emit HCl directly into the atmosphere. It is also important to note that HCl and particulate Cl can be also emitted from agricultural crop residue burning, which is prevalent in northern India during October and November. However, our measurements were carried out during February, which is not the crop residue burning season in northern India.

Chennai. The measurements of aerosol composition, using an Aerodyne aerosol chemical speciation monitor (ACSM) and an aethalometer (AE33), were carried out in Chennai during 5 January 2019 to 5 February 2019, with an aim to complement the Delhi measurements and to cover the festival of Bhogi, so characteristic features associated with rubbish/waste burning could be investigated. Please note, as discussed below, the Bhogi festival is marked by large-scale wood and domestic waste/rubbish burning in this region. Chennai, the fourth most populated city in India (>5 million) is a southeastern coastal urban city and, unlike Delhi, experiences a tropical hot and humid climate with higher temperatures during the measurement period. Daytime average temperatures ranged from 20 °C to 29 °C and relative humidities from 50% to 90%. The sampling was carried out with a dedicated inlet with proper protection from insect and other blockages. The instruments were housed at the Indian Institute of Technology Madras in a temperature-controlled laboratory (12.99° N, 80.23° E; 14 m above sea level). The campaign in Chennai was planned in such a way that the measurements covered the period of a local festival, called Bhogi, which is celebrated in the middle of January (mostly on 14 January), marking the beginning of the Tamil month of Thai, and is one of the biggest and most important festivals in the state of Tamilnadu. In this part of India, it is considered to be even more important and bigger than the festival of Diwali and is celebrated across entire Tamilnadu, including Chennai. Previous researchers have reported air quality deterioration with pollutants exceeding levels well above the standard limits during the Bhogi festival[37]. As a customary and old tradition during this festival, people thoroughly clean their houses and remove all unwanted and unusable goods. Another important ritual, which follows the cleaning, called Bhogi Mantalu, is to throw all unwanted and unusable household items in a fire fuelled by wood and cow-dung cakes as a religious belief. The burning generally starts on the evening of the festival and continues until early morning. During our measurement period, the festival was on 14 January, and as can be seen in Fig. 2b, the NR-PM$_1$ mass concentration reached a peak value of 320 μg m^{-3} (Extended Data Fig. 2) as a result of emissions due to burning. During the entire campaign, sulfate was found to be the second largest mass contributor to the NR-PM$_1$ after organics. During the Bhogi burning, however, particulate chloride was the second largest mass contributor.

Instrumentation. An ACSM[57] was deployed at the Indian Meteorological Department, New Delhi, from 1 February to 3 March 2018, and at the Indian Institute of Technology Madras from 5 January to 5 February 2019 to measure the chemical composition of non-refractory submicron aerosol particles (with vapourization temperature <600 °C), including organics (Org), sulfate (SO_4), nitrate (NO_3), ammonium (NH_4) and chloride (Cl) at high time resolution (about 15 min) and high mass sensitivity. Maintenance and calibration of the instrument were performed before the start of each campaign and once during the campaign as per the normal protocols[58]. For the ambient measurements, briefly, ambient air was drawn through a stainless steel tube and a $PM_{2.5}$ cyclone to remove the coarse mode particles. The air sample was then passed through a silica gel dryer to avoid water condensation in the sampling line before reaching the ACSM inlet, out of which 0.085 l/min (85 cm^{-3}) was isokinetically allowed to pass into the ACSM sampling valve. The particles were sampled into a vacuum chamber through an aerodynamic lens (approximately 2 torr). Then the PM was flash vapourized on a hot surface at around 600 °C and ionized, followed by subsequent detection using a quadrupole mass spectrometer. Theoretically, the concentrations of the chemical species are proportional to the measured ion signal.

The mass calibrations were performed using a TSI electrostatic classifier (SMPS; TSI 3082) as a differential mobility analyser to select the desired particle sizes with ammonium nitrate and ammonium sulfate. The calibration resulted in a response factor of 7.65×10^{-11} with relative ionization efficiency for ammonium of 4.96 and sulfate of 1.08 at Chennai; the values for Delhi were 7.65×10^{-11}, 4.96 and 0.9, respectively. The 3 s.d. uncertainties of ACSM for ammonium, chloride, sulfate, organics and nitrate are 0.284 μg m^{-3}, 0.011 μg m^{-3}, 0.024 μg m^{-3}, 0.148 μg m^{-3} and 0.012 μg m^{-3} respectively for 30 min averages. A default relative ionization efficiency value of 1.3 was used for chloride. Given the unique composition of Delhi PM, the phase state can be different from typical ambient measurements in other environments across the globe where composition-dependent collection efficiency was used[59]. Therefore, a collection efficiency of 0.5 was used throughout, assuming most of the particles to be semi-solid inside the ACSM, in line with previous literature[59]. It is important to note that assumption of non-size-dependent collection efficiency may affect the absolute aerosol mass concentration, whereas the relative mass abundance and hence the hygroscopicity will not change with collection efficiency for internally mixed aerosols.

Thermodynamic modelling. Thermodynamic equilibrium between an NH_4^+–H^+–SO_4^{2-}–NO_3^-–Cl^-–H_2O inorganic PM and its gaseous precursors (NH_3, HNO_3 and HCl) is calculated using the ISORROPIA[44,60,61] model (version II; https://www.epfl.ch/labs/lapi/isorropia/). The ISORROPIA II is a computational efficient and rigorous aerosol thermodynamics model that is widely used in the atmospheric aerosol community. The ISORROPIA II solves thermodynamic equilibrium for either a closed system (that is, forward mode, which takes input of total concentration of both gas and particle phases for each species) or an open system (reverse mode, which takes input of particle-phase concentration for each species). For both modes, the equilibrium state is calculated at given temperature and RH values. The output of ISORROPIA II provides gaseous and particulate mass concentrations for each species, as well as the mass concentration of aerosol liquid water content. For all calculations presented here, we assumed the PM adopted a metastable thermodynamic state.

Here we employed the forward mode of ISORROPIA II to calculate the gas–particle partitioning of chloride. For simulations with consideration of chloride, a fixed total concentration of gaseous and particulate chloride of 25 μg m^{-3} (mass concentration as the form of HCl) was used. Such a high concentration of chloride is necessary to reproduce the observed high PM chloride during morning hours in Delhi. We systematically tested the partitioning behaviours of chloride for a wide range of values of various input parameters, including sulfate concentration, total ammonium, temperature and RH (Fig. 3b,c). We used the reverse mode of ISORROPIA II to calculate the aerosol liquid water content associated with inorganic PM with input of measured aerosol inorganic composition, temperature and RH in Delhi (Fig. 2d). The liquid water content in ISORROPIA II is estimated with the Zdanovskii–Stokes–Robinson mixing rule[62], linking the water uptake of the multicomponent system to the hygroscopicity of each individual electrolyte. For the additional water uptake of organic PM, we assumed a constant hygroscopicity parameter $\kappa = 0.1$[20,63]. The ISORROPIA II model does not consider the effect of surface tension, and the aerosol water activity (a_w) equals RH.

We calculated the aerosol hygroscopic growth and CCN activation for scenarios with and without chloride (Fig. 4a,b). Thermodynamic equilibrium of inorganic PM and its precursor gases was calculated using ISORROPIA II in the forward mode. For both scenarios, we randomly sampled sulfate and nitrate concentrations from measured values during the high chloride high organic period (P1) with replacement (that is, bootstrapping, $N = 1{,}000$), and the mean (±s.d.) values for the resampled population were 4.2 ± 1.8 μg m^{-3} and 5.6 ± 2.9 μg m^{-3} for sulfate and nitrate, respectively. The total ammonium (that is, gaseous + particulate) was randomly sampled from a Gaussian distribution with a mean value of 30 μg m^{-3} and 5 μg m^{-3} s.d. The simulation with chloride included a total chloride concentration of 25 ± 5 μg m^{-3}. In addition to the inorganic species, a non-volatile organic PM of 42.9 ± 27.9 μg m^{-3}, bootstrapped from P1, was added in the multicomponent system, and a hygroscopicity κ value of 0.1 was used in the

calculations of water uptake for organic PM. These values used in the simulations are consistent with the measurements during the high chloride period of Delhi, with uncertainty and variability taken into account (Extended Data Fig. 2). A campaign-averaged temperature of 17 °C in Delhi was used in the simulations. Thermodynamic equilibrium states were calculated for different RH values, and the RH-dependent PM composition for the simulation with chloride is shown in Extended Data Fig. 9. Based on the calculated water uptake for inorganic and organic PM components, we modelled the CCN activation for particles with an initial dry diameter of 100 nm (Fig. 4b). We calculated the hygroscopicity κ value at $a_w = 0.99$ (the upper limit of the ISORROPIA II model) for the mixed inorganic–organic particle. Hygroscopic growth at higher a_w values were extrapolated using this constant κ value. This extrapolation is valid because >99% of chloride partitions to the particle phase at $a_w = 0.99$, and further water uptake at higher a_w values does not significantly enhance the hygroscopicity. A surface tension value of pure water (0.072 N m^{-1}) was used in the calculations of CCN activation.

The inferred HCl gas phase concentration was further used to calculate the ratios of HCl:BC and HCl:OC, which was then used to compare with the same ratio derived from the literature for various types of emission, including open biomass burning, open burning of mixed rubbish and burning of plastic waste[27,28,30,38]. The detailed results in this regard obtained from current measurements and as obtained from the literature for various emission ratios from different types of combustion are shown in Extended Data Fig. 6.

***f*(RH).** Following ref. [18], we derived the measured *f*(RH) of aerosol hygroscopic growth from ambient observations. We selected the period of winter (December to mid-February) to spring (mid-February to March) with high concentrations of chloride reported[2], to investigate the effect of chloride co-condensation. Hourly observations during 2015–2019, including $PM_{2.5}$ from the US Embassy in Delhi (https://www.airnow.gov/), along with visibility and meteorological parameters from the Indira Gandhi International Airport (only 7 km away from the US Embassy, https://www.ncdc.noaa.gov/) were used in the analysis. The $PM_{2.5}$ and visibility observations were well calibrated and quality controlled according to the protocols of the US Environmental Protection Agency[64,65], and the National Oceanic and Atmospheric Administration, National Climatic Data Center[66], respectively. The RH values were calculated from dew point temperature and temperature using the Magnus formula[67]. The periods with wind speed larger than 6.5 m s^{-1} or RH higher than 95% were excluded from analysis, to minimize the uncertainties induced by dust and the low accuracy of the RH sensor under high RH conditions[18]. We projected the data pairs of RH, $PM_{2.5}$ and visibility into eight RH bins (with borders of 30%, 40%, 50%, 60%, 70%, 80%, 85%, 90% and 95%), with more than 400 pairs within each bin. The light-extinction coefficient of aerosol particles was derived from visibility data using the Koschmieder's equation[68]. Then, the mass extinction efficiency for each RH bin, *E*(RH) with units of m^2 g^{-1}, was derived as the slope between the light-extinction coefficient and $PM_{2.5}$ concentration with least squares fit linear regression. By normalizing the *E*(RH) with *E*(30%–40%), we derived the *f*(RH) for each RH bin. The uncertainty of *f*(RH) was estimated using bootstrapping[69] by resampling 1 million times from the observations within each RH bin.

The modelled *f*(RH) was calculated for two scenarios with and without chloride (Fig. 4a). Thermodynamic equilibrium and water uptake were calculated following the methods described in 'Thermodynamic modelling'. Hygroscopicity parameter κ_{chem} values for PM_1 were derived from the modelled chemical composition and water uptake. The chemical composition-derived κ_{chem} was then linked with *f*(RH) following a physical based empirical approach[18,49,70,71]. In this approach, the *f*(RH) was parameterized in the form of κ-Köhler theory[70]:

$$f(\mathrm{RH}) = \frac{1 + \kappa_{\mathrm{opt}} \frac{\mathrm{RH}}{1-\mathrm{RH}}}{1 + \kappa_{\mathrm{opt}} \frac{\mathrm{RH}_{\mathrm{ref}}}{1-\mathrm{RH}_{\mathrm{ref}}}}$$

where RH_{ref} is the reference RH for the dry condition. Here RH_{ref} is defined for RH values below 30%. κ_{opt} is the optical hygroscopicity. The optical based κ_{opt} value for bulk $PM_{2.5}$ can be related to κ_{chem} defined for submicrometer particles using the equation below:

$$\kappa_{\mathrm{opt}} = \kappa_{\mathrm{chem}} \times R_\kappa$$

where the ratio R_κ is determined by the particle number size distribution and chemical composition. The values of R_κ ranged from 0.58 to 0.77 based on ref. [71]. An average value of 0.69 was used in the present study following ref. [18].

Factor analysis. Source apportionment of the OA mass spectra obtained from ACSM for both the sites has been performed using the unconstrained positive matrix factorization (PMF) algorithm implemented in Multilinear Engine (ME-2) developed by ref. [72] utilizing source finder tool (SoFi v4.8) in Igor pro[73]. Further, the PMF is a bilinear unmixing receptor model for factor analysis developed by refs. [72,74] that simplifies the complex datasets to a linear combination of source types and their time-dependent concentration. In PMF, the measured organic mass spectra represented in the form of a matrix X_{mn} (organic mass spectra in *m* rows and ion fragments in *n* columns) is factorized into two sub matrices, the time series G_{mp} and the factor profiles F_{pn}, where *p* is the number of factors/OA sources selected.

$$X = GF + E$$

Here, E_{mn} is the residual matrix containing the fraction of the matrix *X* that is unexplained by the model solution. The model then uses a least square algorithm to minimize the object function *Q* as given in the below equation:

$$Q = \sum_{i=1}^{m} \sum_{j=1}^{n} \left(e_{ij} | \sigma_{ij}\right)^2$$

where e_{ij} represents the squared residuals and σ_{ij} are the respective measurement uncertainties. The extraction procedure of organic mass spectra, corresponding error matrices, time and *m*/*z* values as model input have been adopted from refs. [57,75]. The input data were created up to *m*/*z* 120 and analysed while increasing the number of factors from two to eight. The optimum number of factors was obtained after careful evaluation of several parameters including residuals, time series and Q/Q_{exp} values of various solutions gained by running the model from different initial conditions (SEED run). For Delhi, a five-factor solution profile was found to be the most suitable. The factors were assigned after comparing the mass spectra profiles with some known references from published literature[73] including 1-HOA, 2-BBOA, 3-COA, 4-oxygenated POA (OPOA) and 5-oxygenated OA (OOA).

Similarly, for Chennai, the analysis with a higher number of factors (greater than four) resulted in splitting of identified sources. Thus, the results with the four factors/OA sources HOA, BBOA, semi-volatile/less-oxidized-oxygenated OAs (SV-OOA/LO-OOA) and low-volatile/more-oxidized-oxygenated OAs (LV-OOA/MO-OOA), seemed to be environmentally and mathematically acceptable for the measured data.

STILT model simulations. We used the STILT model, version 2.0, to simulate the transport of an ensemble of 10,000 air particles to the receptor site, 72 h back in time[76]. We performed a total of 1,830 simulations, one for each ACSM measurement instance for available meteorological data. Although the meteorology from the Global Data Assimilation System we use to drive STILT is coarse, at 0.5° × 0.5° spatial resolution, STILT can resample the influence footprint to a finer spatial resolution. STILT-v2.0 uses a Gaussian kernel density estimator with modified vertical dilution in the hyper near field (1–10 km from the receptor) to allocate the influence of air particles according to a user-specified footprint grid, which we define as a regional domain (72–82° E, 23–33° N) at 0.01° x 0.01° spatial resolution. We use the STILT footprints to determine the average sensitivity of the receptor to nearby polluting sources for low Cl and high Cl modes.

Data availability

The NR-PM_1 species from literature shown in Fig. 1 are available in Extended Data Fig. 1. All other data displayed in figures, including concentrations of NR-PM_1 species measured by the ACSM in Delhi and Chennai in this study, and aerosol liquid water modelled by ISORROPIA II, are available in the figshare repository: https://doi.org/10.6084/m9.figshare.13277486. Source data are provided with this paper.

Code availability

The aerosol thermodynamic model ISORROPIA II is available at https://www.epfl.ch/labs/lapi/software/isorropia/. Other codes used in this paper are available from S.S.G. or P.L. upon reasonable request.

References

55. Panwar, R. M. & Ahmed, S. Assessment of contamination of soil and groundwater due to e-waste handling. *Curr. Sci.* **114**, 166–173 (2018).
56. Sharma, G. et al. Gridded emissions of CO, NO_x, SO_2, CO_2, NH_3, HCl, CH_4, $PM_{2.5}$, PM_{10} BC, and NMVOC from open municipal waste burning in India. *Environ. Sci. Technol.* **53**, 4765–4774 (2019).
57. Ng, N. L. et al. An aerosol chemical speciation monitor (ACSM) for routine monitoring of the composition and mass concentrations of ambient aerosol. *Aerosol Sci. Technol.* **45**, 780–794 (2011).
58. Freney, E. et al. The second ACTRIS inter-comparison (2016) for aerosol chemical speciation monitors (ACSM): calibration protocols and instrument performance evaluations. *Aerosol Sci. Technol.* **53**, 830–842 (2019).
59. Middlebrook, A. M., Bahreini, R., Jimenez, J. L. & Canagaratna, M. R. Evaluation of composition-dependent collection efficiencies for the Aerodyne aerosol mass spectrometer using field data. *Aerosol Sci. Technol.* **46**, 258–271 (2012).
60. Nenes, A., Pandis, S. N. & Pilinis, C. ISORROPIA: a new thermodynamic equilibrium model for multiphase multicomponent inorganic aerosols. *Aquat. Geochem.* **4**, 123–152 (1998).
61. Nenes, A., Pandis, S. N. & Pilinis, C. Continued development and testing of a new thermodynamic aerosol module for urban and regional air quality models. *Atmos. Environ.* **33**, 1553–1560 (1999).

62. Stokes, R. H. & Robinson, R. A. Interactions in aqueous nonelectrolyte solutions. I. Solute-solvent equilibria. *J. Phys. Chem.* **70**, 2126–2131 (1966).
63. Liu, P. F. et al. Resolving the mechanisms of hygroscopic growth and cloud condensation nuclei activity for organic particulate matter. *Nat. Commun.* **9**, 4076 (2018).
64. *List of Designated Reference and Equivalent Methods* (EPA, 2015).
65. *Standard Operating Procedure for the Continuous Measurement of Particulate Matter* (EPA, 2009).
66. Lott, N. J. The quality control of the integrated surface hourly database. In *Proc. 14th Conference on Applied Climatology* 7.8 (AMS, 2004).
67. Magnus, G. Versuche über die spannkräfte des wasserdampfs. *Ann. Phys.* **137**, 225–247 (1844).
68. Knowles Middleton, W. E. *Visibility in Meteorology: The Theory and Practice of the Measurement of the Visual Range* (Univ. Toronto Press, 1935).
69. Efron B. T. & Tibshirani, R. J. *An Introduction to the Bootstrap* (CRC Press, 1993).
70. Brock, C. A. et al. Aerosol optical properties in the southeastern United States in summer – Part 1: hygroscopic growth. *Atmos. Chem. Phys.* **16**, 4987–5007 (2016).
71. Kuang, Y. et al. A novel method for deriving the aerosol hygroscopicity parameter based only on measurements from a humidified nephelometer system. *Atmos. Chem. Phys.* **17**, 6651–6662 (2017).
72. Paatero, P. The multilinear engine – a table-driven, least squares program for solving multilinear problems, including the *n*-way parallel factor analysis model. *J. Comput. Graph. Stat.* **8**, 854–888 (1999).
73. Canonaco, F., Crippa, M., Slowik, J. G., Baltensperger, U. & Prevot, A. S. H. SoFi, an IGOR-based interface for the efficient use of the generalized multilinear engine (ME-2) for the source apportionment: ME-2 application to aerosol mass spectrometer data. *Atmos. Meas. Tech.* **6**, 3649–3661 (2013).
74. Paatero, P. & Tapper, U. Positive matrix factorization – a nonnegative factor model with optimal utilization of error-estimates of data values. *Environmetrics* **5**, 111–126 (1994).
75. Sun, Y. et al. Characterization of summer organic and inorganic aerosols in Beijing, China with an aerosol chemical speciation monitor. *Atmos. Environ.* **51**, 250–259 (2012).
76. Fasoli, B., Lin, J. C., Bowling, D. R., Mitchell, L. & Mendoza, D. Simulating atmospheric tracer concentrations for spatially distributed receptors: updates to the Stochastic Time-Inverted Lagrangian Transport model's R interface (STILT-R version 2). *Geosci. Model Dev.* **11**, 2813–2824 (2018).

Acknowledgements

S.S.G. acknowledges partial funding from the Ministry of Earth Sciences (sanction number MoES/16/04/2017-APHH (PROMOTE)), the Government of India, and the Department of Science and Technology (sanction number DST/CCP/CoE/141/2018C), the Government of India. This work was partially supported by the UK Natural Environment Research Council with grant reference numbers NE/P016480/1 and NE/P016472/1. P.L. acknowledges the start-up funding support from Georgia Insitute of Technology. Y.C. was funded under NERC grant number NE/P016405/1. All the authors are grateful to the APHH-PROMOTE team for providing logistic and experimental support during the campaign. Help from V. Kumar Soni, S. Singh and the staff at the India Meteorological Department, Delhi office, is specially acknowledged for logistic support during the campaign and providing the meteorological data. S.S.G. thankfully acknowledges Alfatech Services, New Delhi, for their generous technical support during the campaign. P.L. acknowledges fruitful discussions with N. L. Ng and L. G. Huey. L.J.M. acknowledges helpful discussions with D. Robie. We acknowledge A. Nenes for providing the ISORROPIA II model. U. Panda acknowledges CSIR for fellowship. S.S.G. was a recipient of the Fulbright Fellowship.

Author contributions

S.S.G. and P.L. designed the research. S.S.G., G.M. and H.C. conceptualized and planned the field campaign. U. Panda, S.S.R., A.S., S.M.K. and E.D. carried out the extensive field measurements and collected the ACSM data in Delhi and Chennai. S.S.G., P.L., U. Panda, S.M.K., R.R. and M.L.P. conducted ACSM data analysis. S.S.G., P.L., X.W., J.A., E.R.V. and G.M. conducted the ACSM data interpretation. P.L., S.S. and S.S.G. carried out the thermodynamic model simulations and conducted the data analysis and interpretation. P.L., Y.C., Y.W. and S.S.G. conducted the *f*(RH) and Köhler theory calculations and result intepretations. T.L. carried out the STILT simulations and performed the data interpretation with help from P.L. and S.S.G. S.S.G. and P.L. led the manuscript writing with specific inputs and edits from X.W., L.S., S.T.M., L.J.M., U. Pöschl, G.M., M.O.A. and H.C. All co-authors discussed the results and commented on the manuscript.

Competing interests

The authors declare no competing interests.

Additional information

Extended data is available for this paper at https://doi.org/10.1038/s41561-020-00677-x.

Supplementary information The online version contains supplementary material available at https://doi.org/10.1038/s41561-020-00677-x.

Correspondence and requests for materials should be addressed to S.S.G. or P.L.

Peer review information *Nature Geoscience* thanks Baerbel Sinha and the other, anonymous, reviewer(s) for their contribution to the peer review of this work. Primary Handling Editors: Clare Davis; Rebecca Neely.

Reprints and permissions information is available at www.nature.com/reprints.

Ref. in main text	Location	Notes	Date	NR-PM_1	Cl	SO_4	NO_3	NH_4	Org
10, 12	Ahmedabad 23.0N 72.6E	Entire campaign	Sep - Oct, 2017 (32 days)	15.4	0.2 (1.3)	4.3 (27.9)	0.4 (2.6)	1.5 (9.7)	9.0 (58.4)
		High Cl (Diwali)	Oct 19-20, 2017 (1 day)	49.0	1.9 (3.9)	7.0 (14.3)	1.5 (3.1)	1.6 (3.3)	37 (75.5)
17	Mahabaleshwar 17.92N 73.65E	Entire campaign	Mar 2016 - Feb 2017 (12 months)	7.5	0.1 (1.3)	1.7 (22.7)	0.5 (6.7)	0.8 (10.7)	4.5 (60.0)
2	Delhi 28.5N 77.2E	Entire campaign	Jan 2017 – Mar 2018 (15 months)	97.1	8.6 (8.9)	11.5 (11.8)	10.1 (10.4)	10.0 (10.3)	57.0 (58.7)
14	Kanpur 26.5N 80.3E	Entire campaign	Jan 2016 (31 days)	406.4	19.3 (4.7)	52.3 (12.9)	71.2 (17.5)	46.4 (11.4)	217.2 (53.4)
		High Cl (burning event)	Jan 23-24, 2016 (1 day)	437.4	43.8 (10.0)	38.8 (8.9)	37.4 (8.6)	28.9 (6.6)	288.5 (66.0)

Extended Data Fig. 1 | Summary table for the chemical species of non-refractory particulate matter (NR-PM_1) in India reported in literature. Table shows details about the various locations over India as represented in Fig. 1. Values show the absolute mass concentrations in μg m^{-3} (and fractions in %).

	Delhi			Chennai		
NR-PM1 Species and meteorological parameters	**Entire campaign**	**High Chloride period**	**High Chl period (04:00-09:00)**	**Entire campaign**	**High Cl period**	**High Cl period in (04:00-09:00)**
Org	38.8±32.2 (68.7±12.4)	46.3 ± 36.6 (64.4±12.5)	59.6 ± 35.7 (56.6±13.7)	14.4±17.1 (47.4±13.3)	35.9±52.8 (56.6±14.5)	112.5±65.8 (66.0±9.5)
NO_3	3.6± 2.9 (6.3±3.3)	5.3± 3.2 (7.1±3.6)	6.9±2.0 (6.5±2.9)	1.3± 2.0 (4.5±2.3)	2.6±3.3 (4.1±1.7)	7.8± 2.8 (4.6±1.0)
SO_4	3.9 ± 1.82 (6.7±5.2)	4.2±1.7 (5.7±4.0)	5.2±1.4 (4.9±2.0)	10.1± 7.3 (33.2±12.5)	14.1±2.9 (22.2±15.9)	18.4± 1.9 (10.8±7.8)
NH_4	4.5± 4.0 (7.8±3.8)	6.6± 4.7 (8.9±3.6)	11.3 ±4.9 (10.8±4.1)	3.6±2.7 (11.8±5.7)	6.1± 4.0 (9.7±3.7)	12.5±4.2 (7.3±2.9)
Cl	5.9±9.1 (10.2±7.7)	10.1 ± 11.3 (13.7±8.3)	22.1±13.7 (21.0±8.9)	0.83 ± 2.5 (2.7±2.1)	4.5±9.7 (7.1±4.1)	18.9± 12.8 (11.1±2.7)
$NR\text{-}PM_1$	56.7±42.5	71.2±48.1	105.2±42.5	30.3±28.4	64.3±72.13	170.3±87.1
Temperature (˚C)	18.8	16.5	12.3	24.8	24.4	21.8
Humidity (%)	58.4	58.5	78.4	69.5	64.7	76.9
Wind speed (m/s)	0.6	0.6	0.4	1.3	1.2	0.9

Extended Data Fig. 2 | Summary table for the chemical species in $NR\text{-}PM_1$ measured by the Aerosol Chemical Speciation Monitor (ACSM) in the present study. Values show the mass concentration (μg m^{-3} ± standard deviation) and mass fraction in parentheses (%±standard deviation) of respective non-refractory PM species. Average temperature, humidity, and wind speed are also shown.

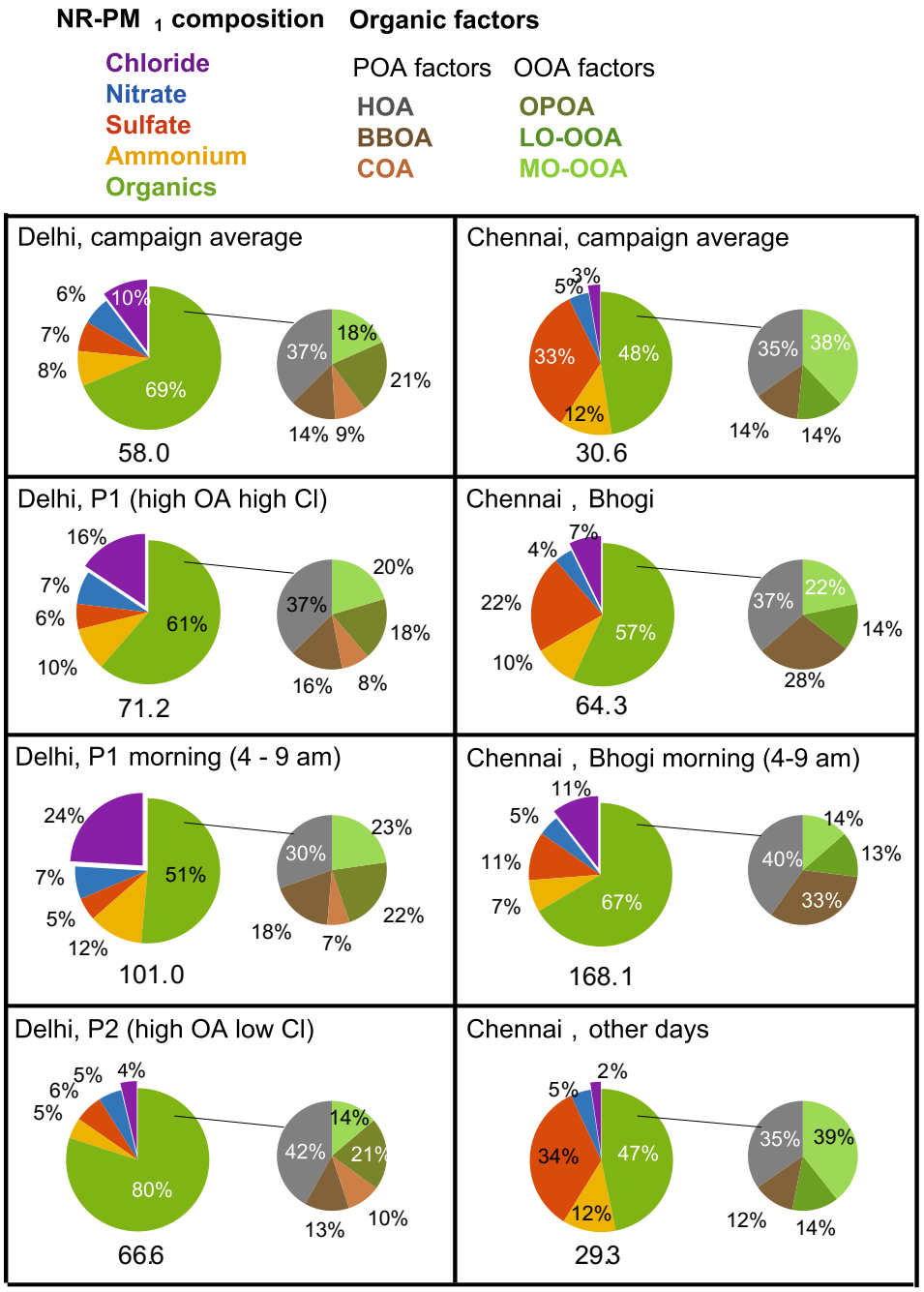

Extended Data Fig. 3 | Distribution of organic and inorganic mass fraction of different chemical species in NR-PM$_1$ and further fractions of different organic aerosol (OA) factors identified by positive matrix factorization (PMF) analysis. The contributions in the form of pie charts are shown for entire campaign, the periods associated with high chloride episode, morning hours (04:00–09:00 am) during the high chloride episode (when partitioning to the particle phase is favourable), and the low chloride days. The left and right panels indicated the fractions for Delhi and Chennai, respectively. The identified primary OA (POA) factors include hydrocarbon-like OA (HOA), biomass burning OA (BBOA), and cooking OA (COA; Delhi only). The identified oxygenated OA (OOA) factors are oxidized primary OA (OPOA; Delhi only), less-oxidized oxygenated OA (LO-OOA; Chennai only), and more oxidized oxygenated OA (MO-OOA). The individual mass fractions (in %) and total NR-PM$_1$ mass is marked in the respective panels.

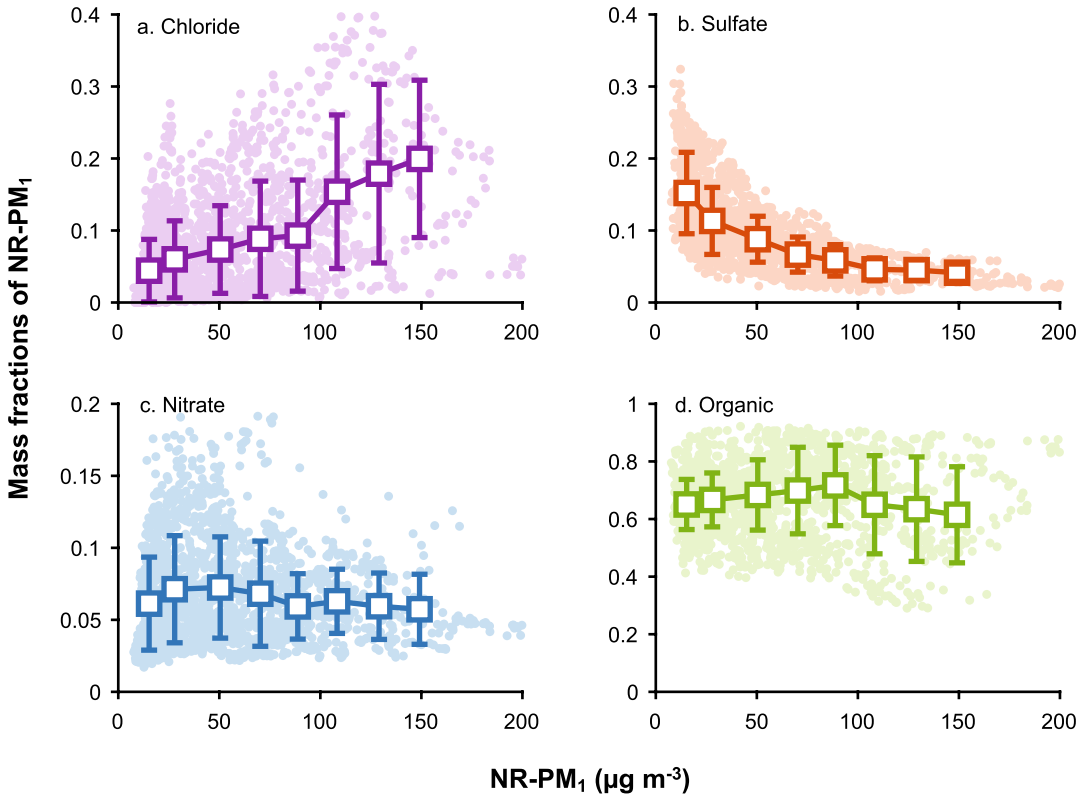

Extended Data Fig. 4 | Scatter plot of mass fraction of NR-PM_1 versus absolute mass of NR-PM_1 (Org, NO_3^-, NH_4^+, SO_4^-, and Cl^-) for Delhi. (**a**) Total NR-PM_1 mass versus chloride mass fraction (**b**) Total NR-PM_1 mass versus sulphate mass fraction (**c**) Total NR-PM_1 mass versus nitrate mass fraction, and (**d**) Total NR-PM_1 mass versus organic mass fraction. The square points in each panel represent the mean values for different concentration bins and the error bars extend from lower to upper standard deviation.

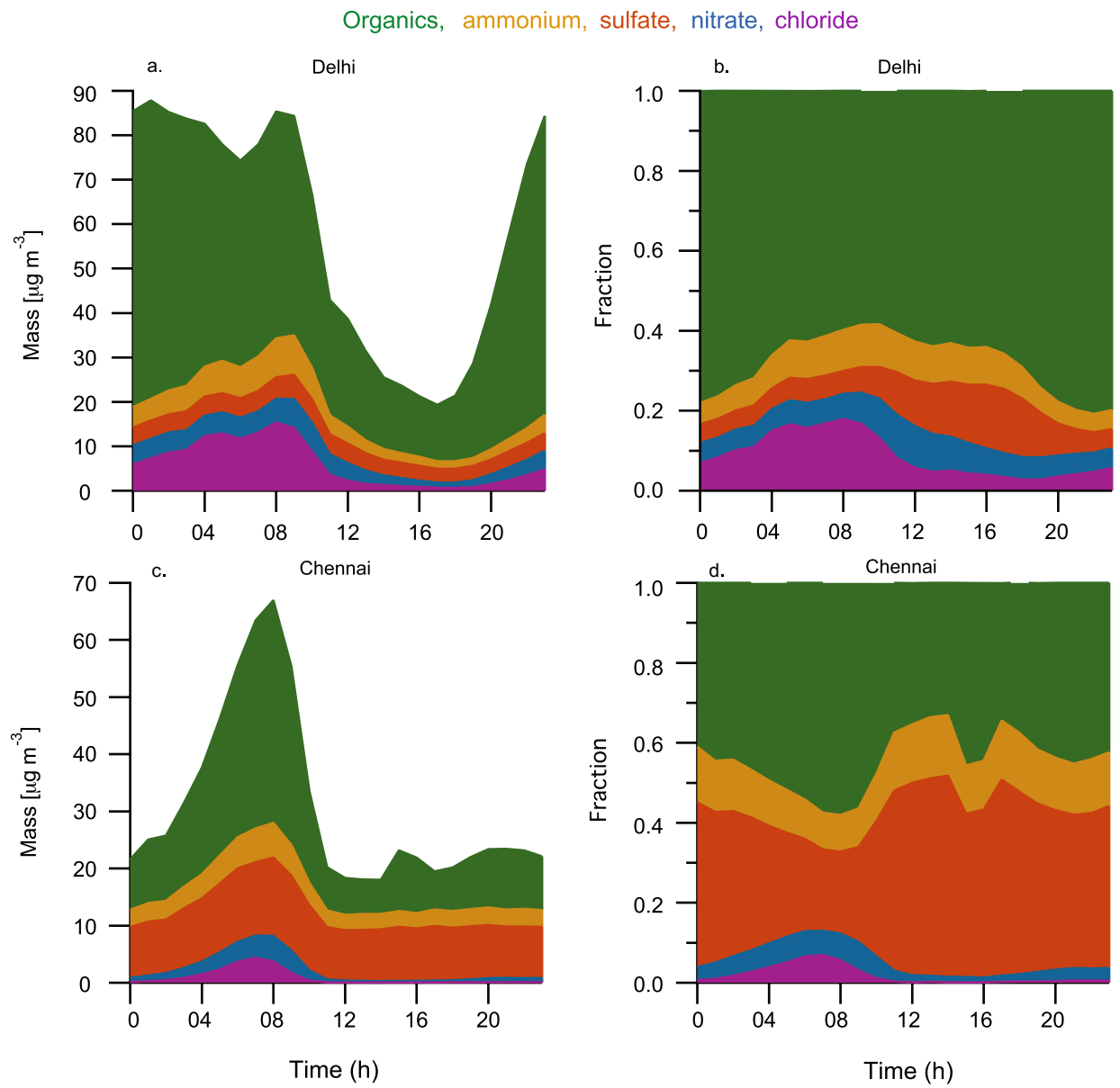

Extended Data Fig. 5 | Averaged diel variations of non-refractory chemical components and respective fraction in submicrometer particulate matter (NR-PM_1; Org, NO_3^-, NH_4^+, SO_4^-, and Cl^-) measured in Delhi and Chennai. (**a**) Stacked diel variations in absolute mass concentrations of chemical components in NR-PM_1 measured by ACSM during the field campaign in Delhi. (**b**) Stacked diel variations in the mass fraction of NR-PM_1 for Delhi as derived from absolute mass concentrations. (**c**) Same as (a) for Chennai. (**d**) Same as (b) for Chennai.

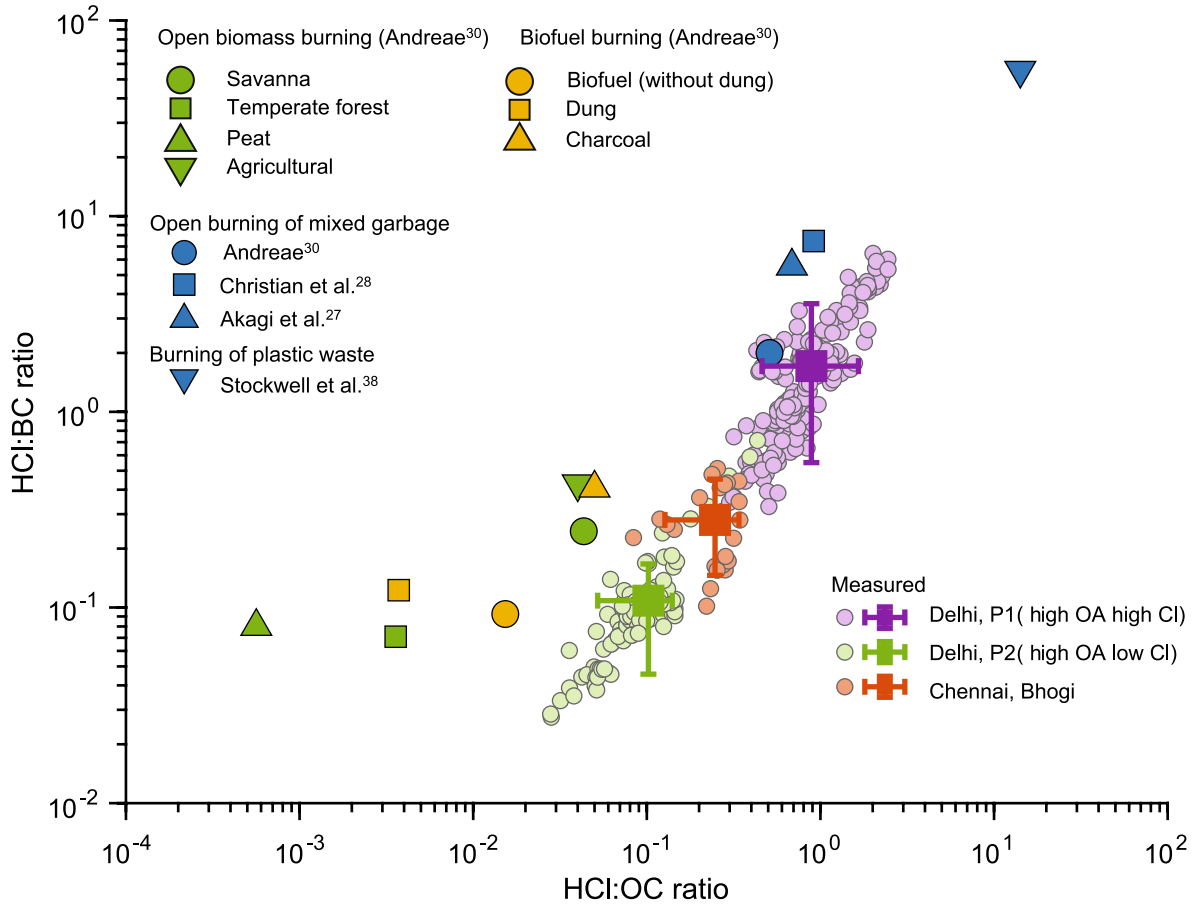

Extended Data Fig. 6 | Scatter plot of HCl:BC versus HCl:OC ratios for various type of burning as collected from literature, compared with measured ratios from the present observations from Delhi and Chennai. The fuels for which the emission ratios are derived includes open biomass burning, biofuel burning, open burning of mixed garbage, and burning of plastic waste. The purple dots and corresponding square in the graph represents the HCl:BC and HCl:OC ratios for Delhi during the entire period and averaged over P1 period, respectively. The green dots and corresponding square are similar like purple colour but for period P2. The orange dots and corresponding square is again similar to purple and green dots but for Chennai representing the Bhogi period. The total HCl concentration was inferred from the particulate chloride observed during early morning hours when HCl was expected to partition into the particle phase. The squares represent the arithmetic mean of measured points during respective periods of measurements for corresponding sites and the error bars extend to the 10th and 90th percentiles.

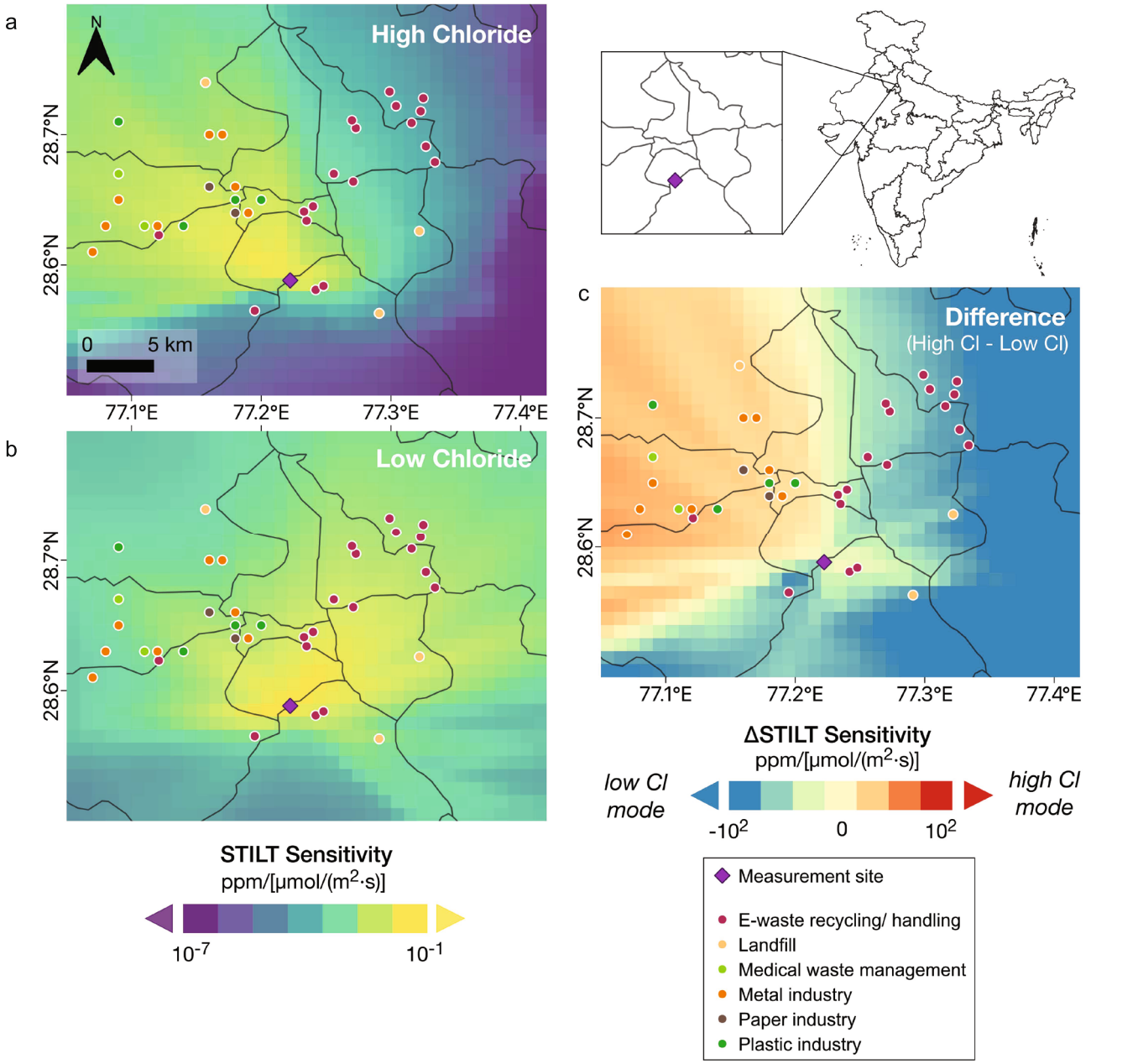

Extended Data Fig. 7 | Sensitivity of the measurement site with respect to nearby potential emission sources. Sensitivity is derived using the Stochastic Time-Inverted Lagrangian Transport (STILT) model. (**a**) Sensitivity during P1: high OA high Cl period, (**b**) for period P2: high OA low Cl period, and (**c**) the difference in the sensitivity between P1 and P2. The map in the upper right corner shows the model domain over the India map. The STILT model was driven by the meteorological data from Global Data Assimilation System (GDAS) with a spatial resolution of 0.5°×0.5°. The corresponding back-trajectory footprints were resampled at a finer resolution of 0.01°×0.01°. Note that the colour bar is in the logarithm scale.

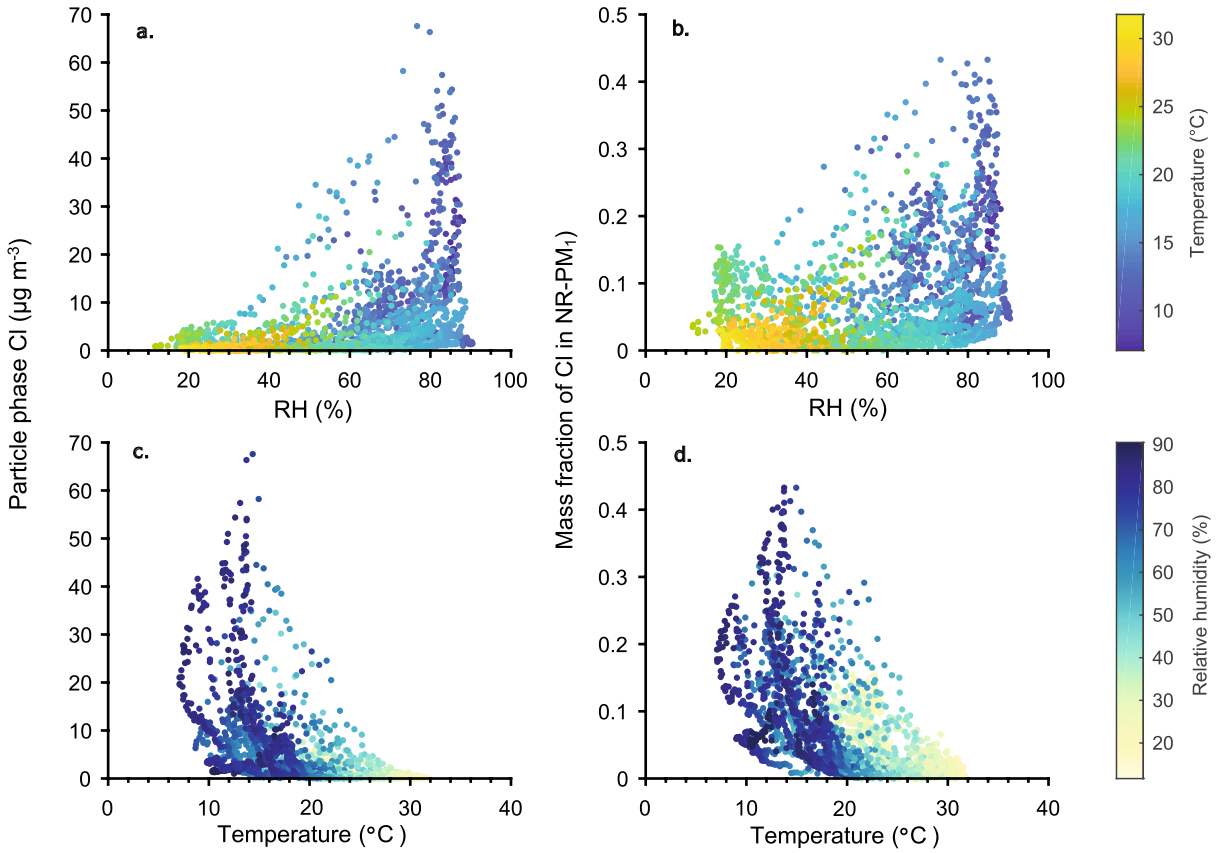

Extended Data Fig. 8 | Scatter plot of relative humidity (RH in %) and temperature (in °C) versus particle phase chloride (µg m^{-3}) and mass fraction of chloride in NR-PM$_1$ over Delhi. (**a**) Mass concentration of particle phase chloride plotted against relative humidity. The data points represented in the scatter plot are scaled by temperature. (**b**) Chloride mass fraction in NR-PM$_1$ plotted versus relative humidity (**c**) same as (a) but plotted against temperature (in °C) and scaled by RH, and (**d**) same as (b) but plotted against temperature (in °C) and scaled by RH.

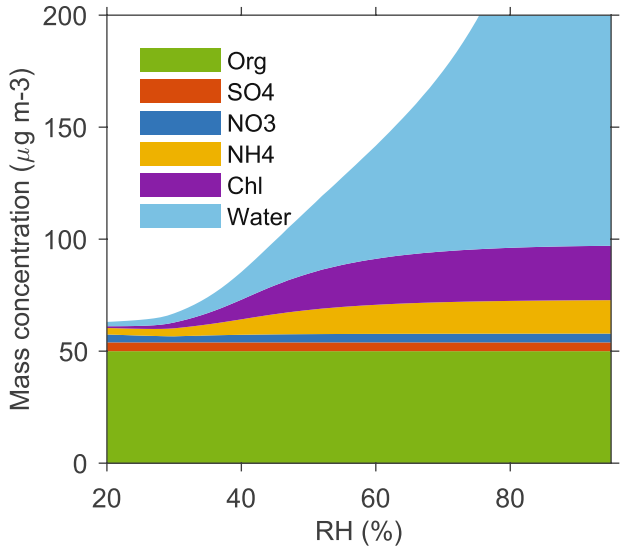

Extended Data Fig. 9 | Mass of organic, inorganic species, and water content as a function of relative humidity. Organic, inorganic mass fraction and water content in NR-PM_1 over Delhi as a function of relative humidity (%) as derived from ISORROPIA model calculations distinctly showing a strong increase in chloride and water contents in NR-PM_1 with increasing relative humidity.